Task Final Report for the
Texas Commission on Environmental Quality

Date: December 30, 2010

Organization: NOAA/NWS/NCEP/Climate Prediction Center

PI: Craig S. Long
Co-I: Kathleen Lantz

Work Order No. 582-8-86246-FY10-07

Project: Interaction of Downward Ultraviolet Radiation with Air Pollution and Clouds

Purpose:

1. **UV and Ozone profile:** Evaluate changes in UV radiometric quantities with redistribution of ozone from the stratosphere to the troposphere by using measured ozone profiles compared with the standard ozone profile used in the TUV radiative transfer code and CAMx air quality model. Use ozone profiles from ozonesondes and Brewer Umkehr retrievals from Houston, TX. Understanding the influence of total ozone and ozone profiles on the variability in UV photolysis rate constants is essential prior to studying the effects of aerosols and clouds on UV.

2. **UV and Aerosols:** Evaluate changes in UV radiometric quantities with aerosol types and aerosol profile shapes compared with the standard aerosol profile and aerosol properties used in the TUV radiative transfer code and CAMx air quality model. Use aerosol properties from measurements in Texas. Understanding the influence aerosol properties and aerosol profiles on the variability in UV photolysis rate constants is essential prior to studying the effects of clouds on UV.

3. **UV and Clouds:** Evaluate changes in UV radiometric quantities with clouds via two aspects. First, we will perform sensitivity studies with TUV to evaluate how cloud layers affect actinic flux in the troposphere. Secondly, we will evaluate the accuracy of NWS MOS cloud forecast products.

1. Introduction

The creation and build up of ozone in the troposphere is the net of multiple reactions. The process begins with the photodissociation of ozone (O_3) itself by ultraviolet light (UV) (i.e. photons of wavelengths less than 320 nm) that generates an oxygen molecule (O_2) and an excited oxygen atom [$O(^1D)$] is given by the photochemical reaction 1:

$$O_3 + hv \rightarrow O_2 + O(^1D) \qquad \textit{(1)}$$

The excited oxygen atom then can react with water vapor to generate a pair of hydroxyl radicals:

$$O(^1D) + H_2O \rightarrow 2OH \qquad \textit{(2)}$$

The hydroxyl radical is central to atmospheric chemistry as it initiates multiple reactions that lead to the formation of tropospheric ozone. As an example, the hydroxyl radical reacts with carbon monoxide to form CO_2 and a hydrogen atom which reacts rapidly with oxygen to form the peroxyl radical HO_2 (other hydrocarbons can react with OH to form organic peroxy radicals RO_2 that result in ozone formation):

$$OH + CO \rightarrow H + CO_2 \qquad \textit{(3)}$$
$$H + O_2 \rightarrow HO_2 \qquad \textit{(4)}$$

Peroxy radicals then go on to react with NO to give NO_2:

$$HO_2 + NO \rightarrow OH + NO_2 \qquad \textit{(5)}$$

NO_2 is photolysed to give atomic oxygen which reacts with molecular oxygen to form tropospheric ozone:

$$NO_2 + hv \rightarrow NO + O \qquad \textit{(6)}$$
$$O + O_2 \rightarrow O_3 \qquad \textit{(7)}$$

The photolysis of ozone is spectrally dependant upon wavelengths in the UV part of the solar spectrum ($\lambda < 320$nm). However, the photolysis of NO_2 is less so at UV wavelengths, but more important in visible wavelengths. This project is focused upon the role UV plays in the formation of tropospheric ozone. As ozone's photodissociation is wavelength dependant to the UV part of the spectrum and NO_2 is not the first section of this task will focus solely upon the photodissociation of ozone. Photolysis for both NO_2 and O_3 are evaluated for sections on the impact of aerosols and clouds on UV radiation.

2. Ozone Photolysis

The ozone photolysis rate constant (sec^{-1}) is calculated from equation 8:

$$j[O_3](\theta,\Omega) = \int_{\lambda_1}^{\lambda_2} F(\lambda,\theta,\Omega)\sigma(\lambda)\phi(\lambda)d\lambda \qquad \textit{(8)}$$

where $\boldsymbol{F}$ is the spectral actinic flux (photons/cm^2/sec/nm) for a given wavelength λ, solar zenith angle θ, and total ozone Ω; σ is the spectral ozone absorption cross section (cm^2/molecule); ϕ is the spectral quantum yield for production of O(^{1}D) (molecules/photon); and λ is the wavelength (nm). Absorption cross-sections and quantum yields are functions of wavelength, and may also be functions of temperature and pressure; they are unique to species and reactions. Laboratory experiments measuring the absorption cross-sections and quantum yields have been conducted for many species that photodissociate in the troposphere. Actinic flux is a radiometric quantity that measures the spectral radiance integrated over all solid angles per unit area. The spherical receiving surface distinguishes the actinic flux from the more commonly measured irradiance, which is the irradiance falling on a horizontal surface. Thus, the actinic flux can be called spherical spectral irradiance. The actinic flux changes with time of day, longitude, latitude, altitude, and season, and is governed by the astronomical and geometrical relationships between the sun and the earth. It is greatly affected by the earth's surface albedo as well as by various atmospheric scatterers and absorbers. Hence, correct model calculation of the temporal and spatial variation of the actinic flux is critical to obtaining accurate photolysis rates for regional and mesoscale episodic photochemical modeling.

3. Effect of Tropospheric Ozone on UV Radiometric Quantities

3.1 Introduction

Throughout this section we will be presenting the % change to photolysis rate constants from using the default US Standard Atmosphere (USSA) ozone profile shape to what is actually observed. As a reference in Figure 3.1 we present profiles of the photolysis rate constant for ozone and NO_2 from the ground up to 50 km for overhead sun and varying total column ozone amounts. In general, the ozone photolysis rate constants are very large in the mesosphere and upper stratosphere above the ozone peak and decrease dramatically below the ozone peak (22 km for the USSA) and are comparatively much smaller, yet nearly constant with height, in the lowest 10 km. The ozone photolysis rate constant profiles show that the greater the total column ozone amount the weaker the photolysis rate constant at a given altitude. Conversely, the photolysis of NO_2 shows hardly any impact due to the amount of total column ozone, and is nearly constant from the mesosphere down to 10 km. Below 10 km, the photolysis rate constant of NO_2 decreases as the surface is approached.

3.2 Sensitivity Tests

Two sensitivity tests were conducted to see how photolysis rate constants would change with a change in the ozone profile shape by placing more ozone in the troposphere to simulate a more polluted tropospheric environment from the USSA standard profile but keeping the total ozone constant; and secondly to move the ozone peak to a different altitude in the stratosphere. The first test would be to vary the surface ozone amount from its default amount of 40 ppb to that from 30 to 300 ppb. Figure 3.2 shows how the ozone profile amounts above the ozonepause were held constant, while below the amounts varied. This way only the varying ozone amounts below the ozonepause impact the photolysis rate constant rates.

Typically, the USSA ozone profile is scaled to the given or forecasted total ozone. Figure 3.3 shows how the USSA ozone profile shape would change as varying total column ozone amounts

were distributed equally throughout the entire profile. The USSA ozone profile has a total ozone amount of 349 DU, and is shown as the profile with the thick black line. Figure 3.3 shows the various ozone profiles for total column ozone amounts from 200 to 500 DU. Figure 3.3 also shows that significantly varying the total column ozone amount does not translate into significant surface ozone amount differences. The surface ozone amount for a total column ozone amount of 200 and 500 DU are 23 and 57 ppb, respectively, or -17 and +17 ppb from the USSA amount of 40 ppb at the surface.

Table 3.1 - TUV USSA Standard profile (349 DU): Tropospheric ozone values when the normalized USSA ozone profile is adjusted to the given total ozone amount.

Total Ozone [DU]	Surface ozone [ppb]
200	23
220	25
240	27
260	30
280	32
300	34
320	37
340	39
349 (default)	40
360	41
380	43
400	45
420	48
440	50
460	53
480	55
500	57

The second sensitivity test was to see how varying the height of the ozone profile peak impacted the photolysis rate constants. The USSA ozone profile has a peak at 22 km. The actual ozone profile peak varies with latitude, and season. Figure 3.4 shows the default USSA ozone profile with its peak amount at 22 km and ozone profiles used for this test with peak profile positions at 24, 26, and 28 km. The total column ozone amount for each profile was held constant as the peak height was repositioned.

3.2.1 Radiative Transfer Calculations

Radiative transfer calculations were performed using the TUV radiative transfer model: TUV-RTM (Madronich 1992). UV spectral actinic flux (300 - 420 nm) was calculated for solar zenith angles 0-90º at 5 degree increments. Photolysis rate constant $j(O_3)$ and erythemally weighted

solar irradiance were also calculated as a function of solar zenith angle. Radiometric quantities were calculated for the surface and as a function of altitude in the troposphere from 1 – 10 km. Radiometric quantities were compared to the same quantity when using the USSA default profile in the RT Code TUV.

3.2.2 Sensitivity Test Results

Figure 3.5 shows the percent change to the ozone photolysis rate constant as the modeled surface ozone is increased from 30 – 300 ppb. The additional tropospheric ozone causes the total ozone to increase, therefore the default profile with 40 ppb of tropospheric ozone is scaled to match the total ozone to remove the effect of total ozone and investigate the effects of a change in tropospheric ozone, which causes an increase in the surface ozone in the default profile from 21-56 ppb. Therefore, the change in the surface ozone is from -9 ppb to +234 ppb from the scaled default profile. The graph indicates that a surface ozone amount that is larger than the default 40 ppb will result in a decrease in the photolysis rate constants at the surface. A 25% increase from 40 to 50 ppb (+10 ppb) has a larger than -5% change to the photolysis rate constants. Nearly doubling the surface ozone amount from 43 to 90 ppb (+47 ppb) has just less than -20% change to the photolysis rate constant. A tripling of the surface ozone amount from 46 to 130 ppb (+84 ppb) has slightly less than a -30% change to the photolysis rate constant. Alternatively, a surface ozone amount decrease from 20 to 21 ppb (-9 ppb) results only in a slight increase of 1-2 % in surface the photolysis rate constant. Three observations can be drawn from this figure: 1) as the positive change to surface ozone increases, the percent change impact decreases; 2) a decrease to surface ozone has much lesser % change than an equally large increase to the surface ozone; 3) percent change amounts are the same for all but extreme solar zenith angles.

Figure 3.6 shows the impacts to the surface ozone photolysis rate constant by changing the altitude of the ozone profile peak position from the default of 22 km to 24, 26 and 28 km. Increasing the height of the ozone profile peak does increase the surface ozone photolysis rate constant. However, the increase is very small (1-2 %) at high sun but becomes a more important effect at zenith angles beyond 60 degrees.

3.4 Total Ozone and Surface Ozone Climatology

As background information the annual total column ozone and surface ozone cycle for the Houston area are presented. Figure 3.7 presents four years of daily NEUBrew total column ozone observations and are compared with Aura OMI satellite observations. Their agreement is to within 5 DU. The annual peak total ozone value occurs in the late May or early June and ranges between 300 and 350 DU. The annual minimum total column ozone value occurs in late December or early January and ranges between 230 and 250 DU. So during the peak surface ozone time period of late spring through early fall, the total column ozone over Houston is in its maximum phase.

A time series of the tropospheric ozone column amounts detected by the NEUBrew Umkehr method is presented in Figure 3.8. Daily average tropospheric ozone (DU) is derived from the lowest altitude of the Umkehr Ozone Solution Profile. Data from only 'good' profiles are used as points in this time series. The oldest data available dates to approximately August 2006. Of interest is how the minimum ozone concentrations occur in the autumn and peak values occurs in the spring. There are several possible causes but is beyond the scope of this paper [Cooper et al., 2006; 2010]. The lack of observations in the winter months is due to the higher frequency of cloudy days.

3.5 Comparisons with Ozone Observations

In the following section we will perform similar comparisons as in the sensitivity tests, but with observed ozone profiles from various ozonesonde campaigns in the Houston area. Each campaign will be characterized to provide the mean ozone profile and its surface ozone amount and the range of all the ozonesonde profiles with altitude. Most ozonesondes do not provide useful information above 30 km. We will determine the maximum altitude for each campaign's set of profiles and then append the USSA profile normalized to match the ozone concentration at the top of each observed profile so as to extend all the profiles up to 70 km where the ozone concentration is assumed to be zero. The total ozone amount for mean, maximum and minimum ozonesonde profile will be determined and compared to the equivalent total ozone profile determined in the second sensitivity test. These observed ozonesonde profiles will differ from the USSA ozone profiles by the total column ozone amount, the location of the peak ozone amount, and the surface ozone amount. Table 3.2 provides a summary of the surface ozone amount and the peak ozone profile altitude for the three sensitivity studies and for the three campaigns used in this study. For our comparisons, as is done in practice, the USSA ozone profile will be adjusted to match the observe ozonesonde total column ozone amount (see Figure 3.3). Table 1 provides the various surface ozone amounts for the adjusted total column ozone amounts.

The final evaluation will be to see how the photolysis rate constants change with altitude in the comparison between the USSA ozone profile and the observed ozone profiles. This should provide guidance as to whether the % changes vary with altitude.

Table 3.2 - Tropospheric ozone range and average peak ozone position**:**

Data-set	Surface Ozone [ppb]	Peak Ozone [km]
USSA standard profile	40 ppb	22
USSA simulated profiles	40 ppb	24, 26, 28
USSA simulated profiles	30 – 300 ppb	22
GMD ozonesondes (24 profiles)	30 – 113 ppb	25.2
INTEX ozonesondes (29 profiles)	21 – 72 ppb	25.9
NEUBrew (807 profiles)	19 – 69 ppb	23

3.5.1 Ozonesonde Campaign Data Sets Used

1) Ozone profiles from ozonesondes from NOAA/ESRL/Global Monitoring Division (GMD) group in Houston, TX. There are 24 ozonesondes from August 19 – September 14, 2000. The mean profile along with the observed range of concentrations with altitude is presented in Figure 3.9.
2) Ozone profiles from ozonesondes from Dr. Gary Morris of Valparaiso University in Houston, TX during IONS-2004 (26 profiles between June – Aug 2004), INTEX-B (23 profiles between March-September 2006). The mean profile along with the observed range of concentrations with altitude is presented in Figure 3.10.

3) Ozone profiles from NEUBrew Network (NOAA/EPA UV Brewer Network) at Houston, TX. Brewer spectrophotometer measurements of total ozone, Umkehr ozone profiles, and tropospheric ozone column. Data extends from August 2006 – present. The mean profile along with the observed range of concentrations with altitude is presented in Figure 3.11.

3.5.2 Comparison Results at the Surface

Percent changes to the surface ozone photolysis rate constant for each campaign (GMD, INTEX/IONS, and NEUBrew Umkehr) are presented in Figures 3.12, 3.13 and 3.14, respectively. In Table 3.3 each campaign's mean, minimum, and maximum total column ozone is provided along with the associated surface ozone for the profiles for each of those cases. Using Table 3.1, the adjusted surface ozone amount is determined, and the difference between the observed and the adjusted surface ozone amount is determined. In Figure 3.12, the % change to the surface ozone photolysis rate constant between the USSA ozone profile adjusted to the mean, maximum, and minimum GMD ozone profiles' total column ozone is presented. The mean GMD campaign ozone profile has a total column ozone amount of 308 DU with a surface ozone amount of 55 ppb. The adjusted USSA ozone profile has a surface ozone amount of about 35 ppb. Hence, the net change in surface ozone is about +20 ppb. This will result in a decrease in the surface ozone photolysis rate constant. The peak ozone altitude for the GMD campaign averaged around 25.5 km (see Table 3.2), which should result in a slight increase in the surface ozone photolysis rate constant. The net effect is about a 4% decrease in the surface ozone photolysis rate constant. The GMD campaign's maximum total column ozone amount was 356 DU with a surface ozone amount of 113 ppb. The adjusted USSA ozone profile for 356 DU has a surface ozone amount of 41 ppb. The surface ozone difference is then +72 ppb. The computed impact between the adjusted USSA ozone profile and the observed maximum profile is a decrease of about 8% to the surface ozone photolysis rate constants. The minimum GMD campaign ozone profile had a total column ozone amount of 259 DU with a surface ozone amount of 30 ppb. The adjusted USSA ozone profile for 259 DU has a surface ozone amount of 30 ppb. The surface ozone difference is then +0 ppb. The surface ozone photolysis rate constant is about 2% greater for this comparison.

Table 3.3 – Mean, minimum, and maximum total column ozone and surface ozone amount for each campaign, the adjusted USSA profile and the difference**.**

	Total Column Ozone (DU)			Surface Ozone Amount (ppb)								
Campaign	Mean	Min	Max	Mean Obs	Min Obs	Max Obs	Mean Adj USSA	Min Adj USSA	Max Adj USSA	Mean Diff	Min Diff	Max Diff
GMD	308	259	356	55	30	113	35	30	41	+20	±0	+72
INTEX/IONS	307	229	406	41	21	71	35	26	46	+6	-5	+25
NEUBrew	283	176	444	38	29	69	32	31	50	+6	-2	+19

In Figure 3.13, the percent change to the surface ozone photolysis rate constant between the USSA ozone profile adjusted to the mean, maximum, and minimum INTEX/IONS ozone profiles' total column ozone is presented. The mean INTEX/IONS campaign ozone profile has a total column ozone amount of 307 DU with a surface ozone amount of 41 ppb. The adjusted USSA ozone profile has a surface ozone amount of about 35 ppb. Hence, the net change in surface ozone is about +6 ppb. This will result in a decrease in the surface ozone photolysis rate constant. The peak ozone altitude for the INTEX/IONS campaign averaged around 25.9 km (see Table 3.2), which should result in a slight increase in the surface ozone photolysis rate constant. The net effect is about a 2% decrease in the surface ozone photolysis rate constant. The INTEX/IONS campaign's maximum total column ozone amount was 406 DU with a surface ozone amount of 71 ppb. The adjust USSA ozone profile for 406 DU has a surface ozone amount of 46 ppb. The surface ozone difference is then +25 ppb. The computed impact between the adjusted USSA ozone profile and the observed maximum profile is a decrease of about 5% to the surface ozone photolysis rate constants. The minimum INTEX/IONS campaign ozone profile had a total column ozone amount of 229 DU with a surface ozone amount of 21 ppb. The adjusted USSA ozone profile for 229 DU has a surface ozone amount of 26 ppb. The surface ozone difference is then -5 ppb. The surface ozone photolysis rate constant is about 2% greater for this comparison.

In Figure 3.14, the % change to the surface ozone photolysis rate constant between the USSA ozone profile adjusted to the mean, maximum, and minimum NEUBrew ozone profiles' total column ozone is presented. The mean NEUBrew campaign ozone profile has a total column ozone amount of 283 DU with a surface ozone amount of 38 ppb. The adjusted USSA ozone profile has a surface ozone amount of about 32 ppb. Hence, the net change in surface ozone is about +6 ppb. This will result in a decrease in the surface ozone photolysis rate constant. The peak ozone altitude for the NEUBrew campaign averaged around 23 km (see Table 3.2), which should result in no increase in the surface ozone photolysis rate constant. The net effect is about a no change in the surface ozone photolysis rate constant. The NEUBrew campaign's maximum total column ozone amount was 444 DU with a surface ozone amount of 69 ppb. The adjusted USSA ozone profile for 444 DU has a surface ozone amount of 50 ppb. The surface ozone difference is then +19 ppb. The computed impact between the adjusted USSA ozone profile and the observed maximum profile is a decrease of about 1% to the surface ozone photolysis rate constants. The minimum NEUBrew campaign ozone profile had a total column ozone amount of 276 DU with a surface ozone amount of 29 ppb. The adjusted USSA ozone profile for 276 DU has a surface ozone amount of 31 ppb. The surface ozone difference is then -2 ppb. The surface ozone photolysis rate constant is about 1% greater for this comparison.

3.5.3 Comparison Results at Various Altitudes

The ozone profile shape in the troposphere differs between each of the campaigns and the USSA ozone profile. We now examine how the ozone photolysis rate constants differ above the surface. In Figures 3.15, 3.16, and 3.17 we present the percent change of the ozone photolysis rate constant for the ozone profiles associated with the mean, minimum and maximum total column ozone amounts for each campaign from the adjusted USSA ozone profile at 2, 4, 6 and 8 km above the surface. In Figure 3.15 at 2 km similar percent changes are determined as were determined at the surface. At higher altitudes, the percent change for all three cases becomes more positive. The increase in percent change for the maximum total ozone profile is larger at higher altitudes than the mean and minimum total ozone profiles. Hence, at 8 km the percent

change of the maximum total ozone profile is largest with a value of nearly +10%. The % change of the mean and minimum total ozone profiles are nearly the same at +7% at 8 km. The above percent changes are for over head sun (0º solar zenith angle). As the solar zenith angle increases the mean and maximum percent change also increases. Beyond 70º solar zenith angle complexities arise when the sun angle becomes below the ozone peak.

Similar findings occur with the INTEX/IONS mean, minimum, and maximum total ozone profiles in Figure 3.16. However, the magnitude of the difference of the surface ozone amount for the mean and maximum cases are not nearly as large as in the GMD campaign. As a result, the increase in the percent change with altitude for these cases is not as great as that for the GMD campaign. The minimum total ozone case is nearly identical to that of the GMD campaign and produces similar results.

Figure 3.17 shows that because the adjusted USSA surface ozone amounts and the observed NEUBrew mean, minimum, and maximum case are not very large, the percent change for each case is not large. This result continues to exist above the surface. An increase of the percent change for all three cases as the altitude increases. But this increase is much smaller than that for the other two campaigns.

Further investigation as to why the percent change in ozone photolysis rate constants increase with altitude between the adjusted standard profile and the observed ozonesonde profile reveals that not only are the peak ozone amounts higher for the three campaigns, but also the ozonepause is higher. The standard profile ozonepause is near 10 km, which is about 5 km lower than the ozonepause observed in the three campaigns. Additionally, the observed ozone concentration at the ozonepause is smaller than the standard profile. As a result the standard profile will have more ozone lower in the atmosphere than that observed. The observed photolysis rate constants are then greater in the upper troposphere than what would be computed by using the standard profile.

3.6 Summary

Previous literature has concentrated primarily on the effect of ozone redistribution from the stratosphere to the troposphere on either UV solar irradiance or erythema and very few have evaluated the effect of changes in the ozone profile on actinic flux or photolysis rate constant constants except a few studies (e.g. Kazantzidis 2005; Bruhl and Crutzen, 1989). Previous studies have concentrated primarily on regions of the world outside the U.S. The work here uses ozone profiles specifically from Texas and compares to the standard profile used in the TUV Radiative Transfer Model and the CAMx model.

The effect of changes in the ozone profile from the standard ozone profile has very little effect on $j(NO_2)$ of less than 0.5%. Larger effects are seen in shorter wavelengths of actinic flux and in $j(O_3)$. Changes in $j(O_3)$ will affect the concentration of the hydroxyl radical in the atmosphere and therefore the oxidative capacity of the atmosphere. Evaluating changes in the hydroxyl radical and its effect on tropospheric ozone concentrations was outside the scope of this investigation.

Sensitivity tests showed that increasing the surface ozone amount while keeping the stratospheric amount constant results in decreasing the ozone photolysis rate constant at the surface. A 10 ppb increase in surface ozone decreases the ozone photolysis by 5%. An increase of 25 ppb decreases the ozone photolysis by about 12% and an increase of 47 ppb decreases the ozone

photolysis by nearly 20%. Another sensitivity test showed that if the ozone peak is higher than the standard profile's by 2 to 6 km, there is a 1-2% increase in the ozone photolysis rate constant.

In practice, the standard profile is equally adjusted to match the expected total column ozone amount. Comparisons of the surface ozone photolysis rate constants between the mean, minimum, and maximum ozonesonde profiles for three campaigns against the adjusted standard profiles agree with the findings from the sensitivity tests. That is when ozonesonde profiles had smaller surface ozone amounts than the adjusted standard profiles; the ozone photolysis rate constant at the surface also was smaller. Alternatively, when ozonesonde profiles had greater amounts of surface ozone than the adjusted profiles; the ozone photolysis rate constant at the surface was also larger. The % change also seems to be a function of the percent increase of the surface ozone amount.

Examination of how the percent change of the ozone photolysis rate constant varied at different altitudes revealed that higher above the surface the ozone photolysis rate constants for the ozonesondes from the three campaigns were greater than that determined from the adjusted standard profile. The likely cause for this is that the ozonepause of the standard profile is near 10 km, while the ozonepause for all three campaigns averaged near 15 km.

3.7 Conclusions

Usage of the standard ozone profile in computations of ozone photolysis rate constants will slightly underestimate by 1-2% the photolysis rate constants for small surface ozone amounts and will overestimate the surface photolysis rate constants by 2-8% for larger amounts of surface ozone. In the vertical, the standard ozone profile has the ozonepause 5 km lower than observations for the Houston area. As a result, usage of the standard profile will increasingly underestimate the ozone photolysis rate constants by a maximum of 0-10% at 8 km.

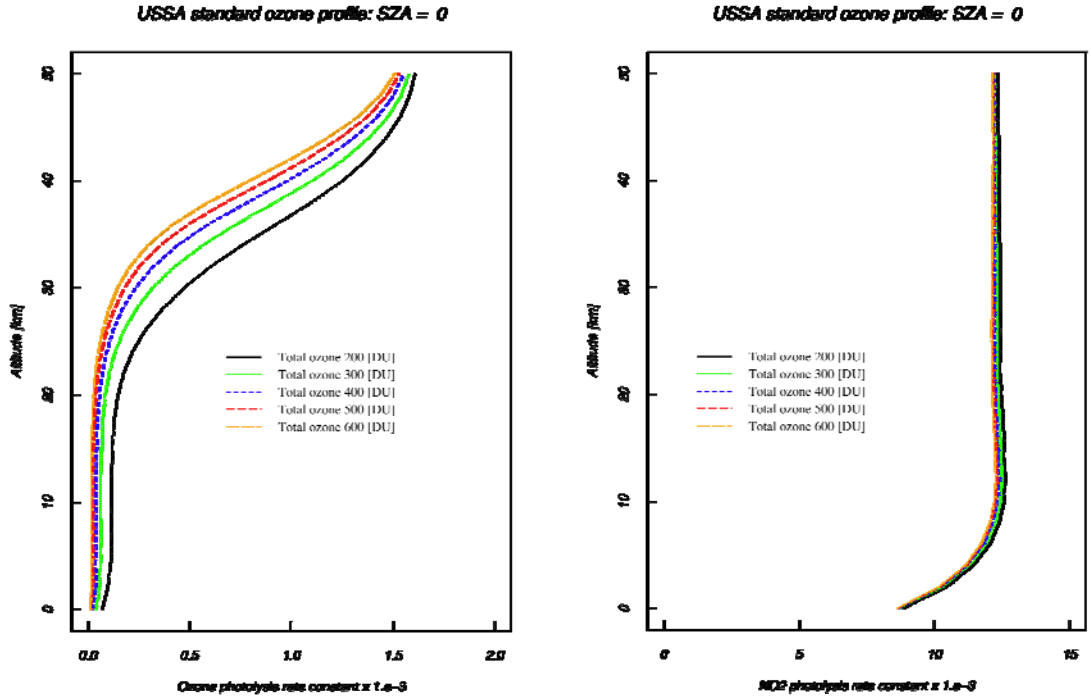

Figure 3.1: Vertical profiles of photolysis rate constants for ozone (left) and NO_2 (right) from the surface to 50 km for different total column ozone amounts from 200 to 600 DU assuming the US standard atmospheric ozone profile shape with a solar zenith angle of 0 degrees.

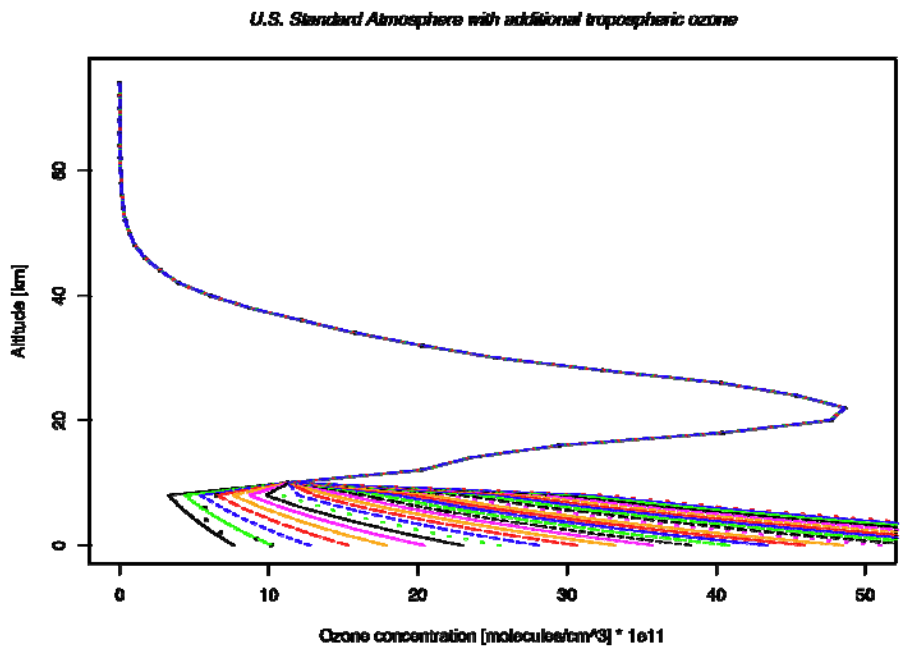

Figure 3.2: Ozone altitude profiles used for tropospheric ozone sensitivity tests on $j(O_3)$. The USSA ozone profile shape is used with varying amounts of tropospheric ozone from 30 – 300 ppb at the surface. The USSA pressure table was used for the calculations to parts per billion. The USSA ozone profile used as the default in the RT code TUV is given in the black dots with a surface tropospheric ozone amount of 40 ppb.

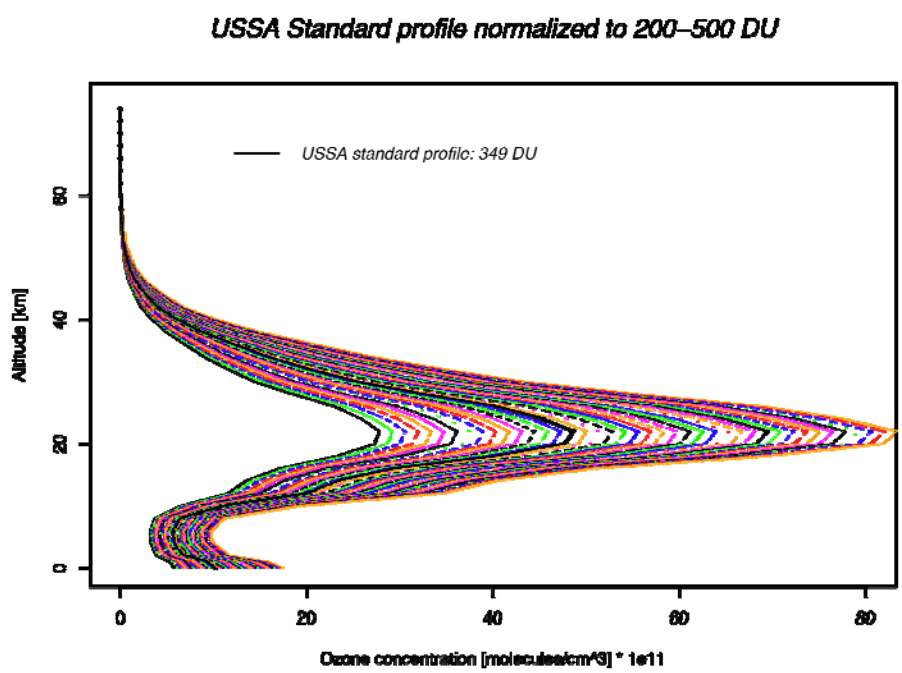

Figure 3.3: USSA standard ozone profiles normalized to different total column ozone amounts. Each profile is used for the comparison for the profiles in Figure 3.2, where the total column ozone for the Figure 3.3 is matched to the total ozone in Figure 3.2. The USSA ozone profile normalized to total column ozone amounts of 200 – 500 DU gives surface ozone values of 23 – 57 ppb (see Table 2). The USSA pressure table was used for the calculations to parts per billion. The USSA ozone profile used as the default in the RT code TUV is given in the thick black line with a surface tropospheric ozone of 40 ppb and total ozone of 349 DU.

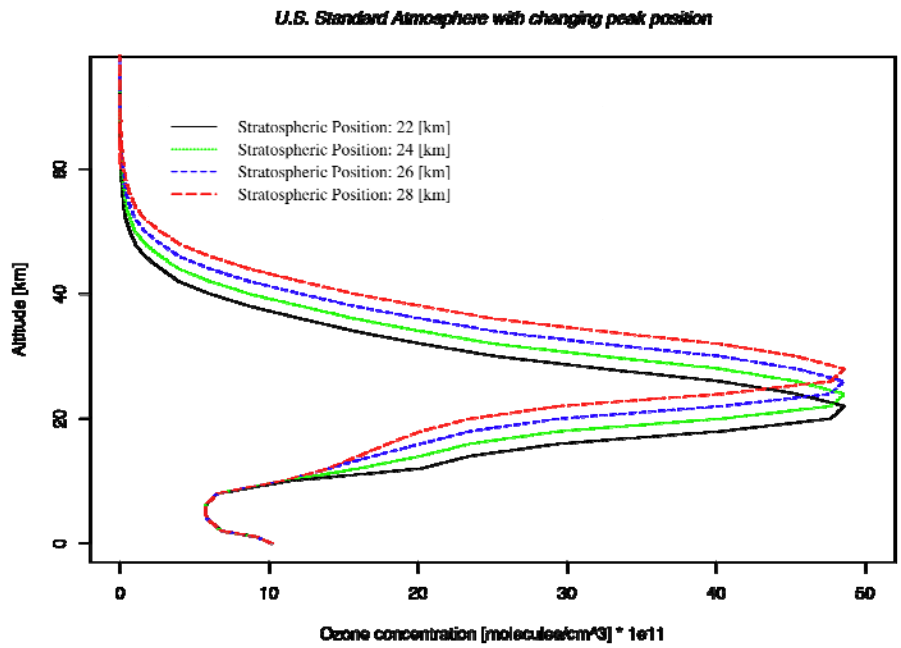

Figure 3.4: Ozone altitude profiles used for stratospheric ozone peak position sensitivity tests on $j(O_3)$. The USSA ozone profile is used with the peak in total ozone changed from 22 km to 28. The USSA ozone profile used as the default in the RT code TUV is given in black with the total ozone peak at 22 km.

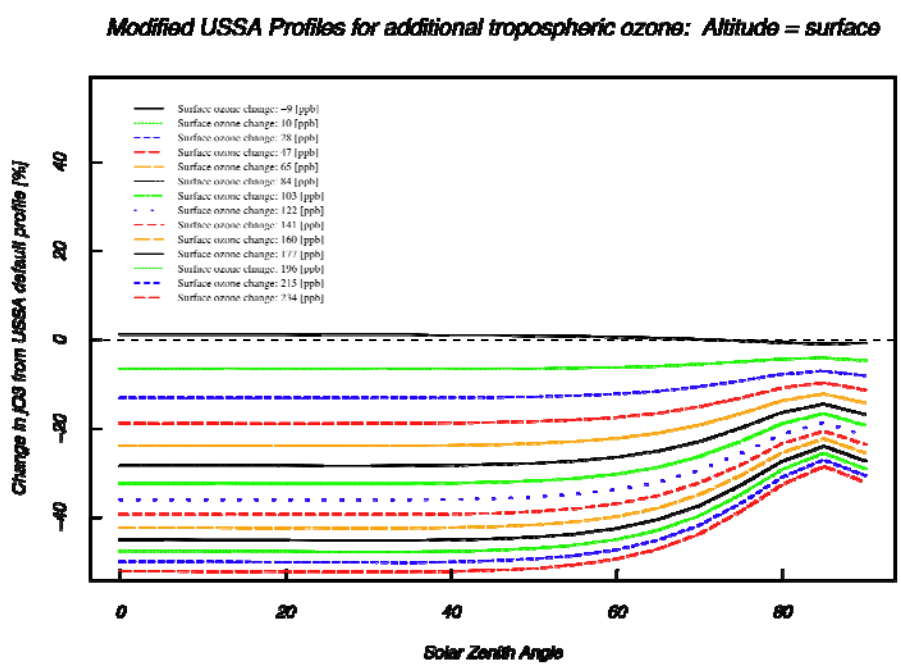

Figure 3.5: Surface $j(O_3)$ using modified USSA ozone profile (with additional tropospheric ozone) compared to $j(O_3)$ using default profile of the USSA.

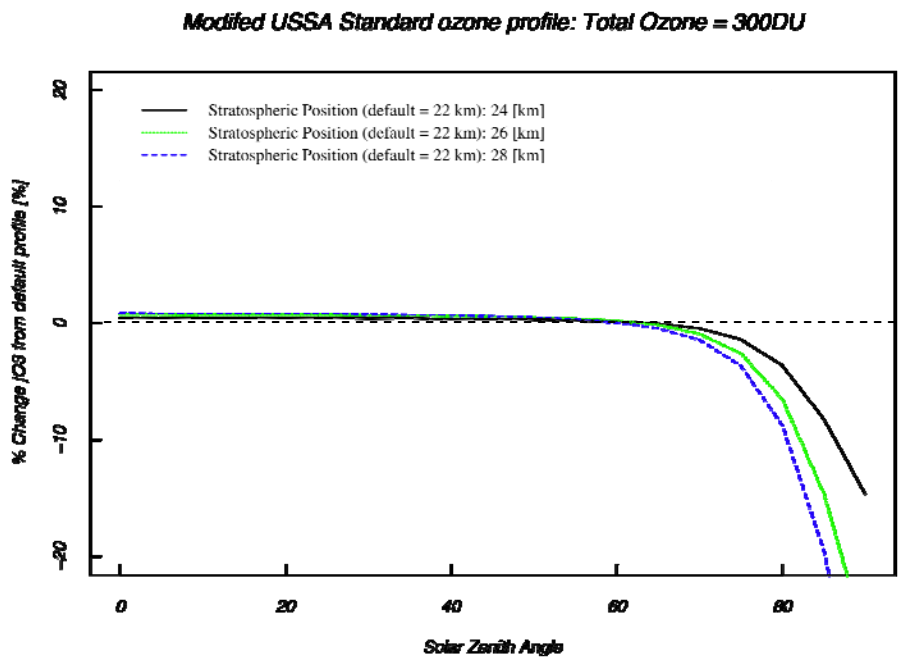

Figure 3.6: Surface $j(O_3)$ using modified USSA ozone profile with changing peak ozone position (24 – 28 km) compared to USSA ozone profile (22 km).

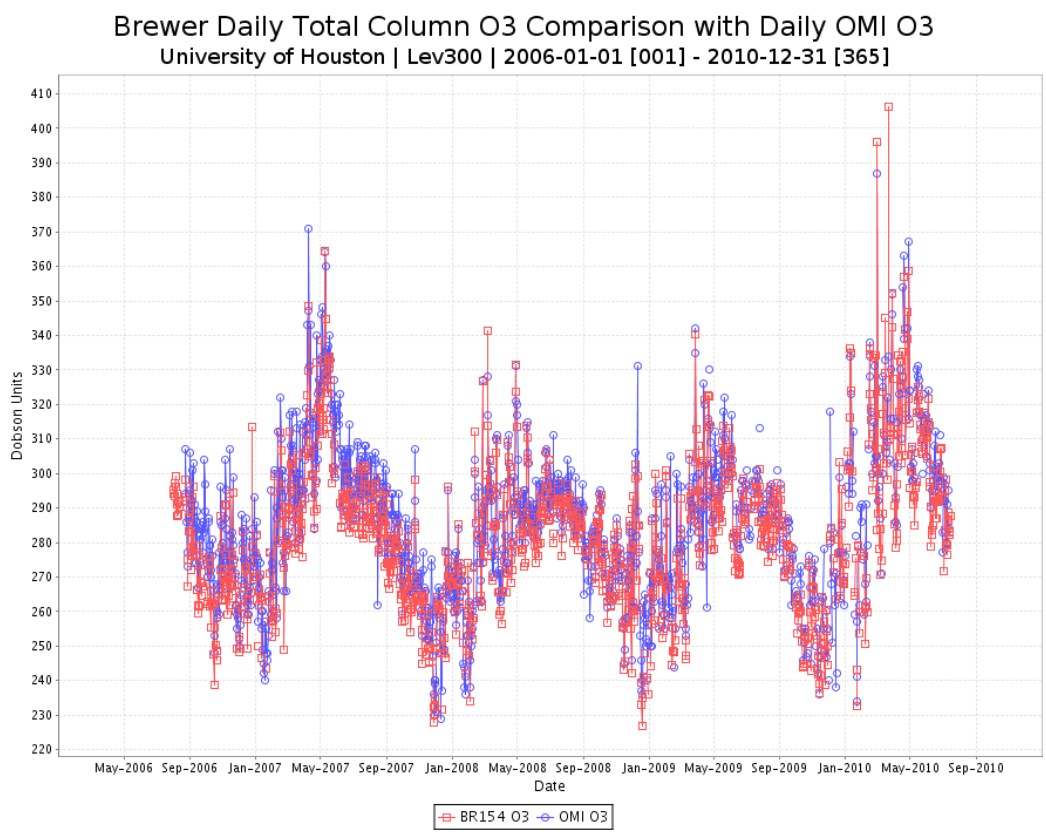

Figure 3.7: NEUBrew total column ozone amounts (DU) (red) at the University of Houston from August 2006 to Present. Aura OMI satellite total column ozone amounts (blue) are over-plotted to show agreement. Peak total ozone amounts occur in late May or early June, while minimum total ozone amounts occur in late December or early January.

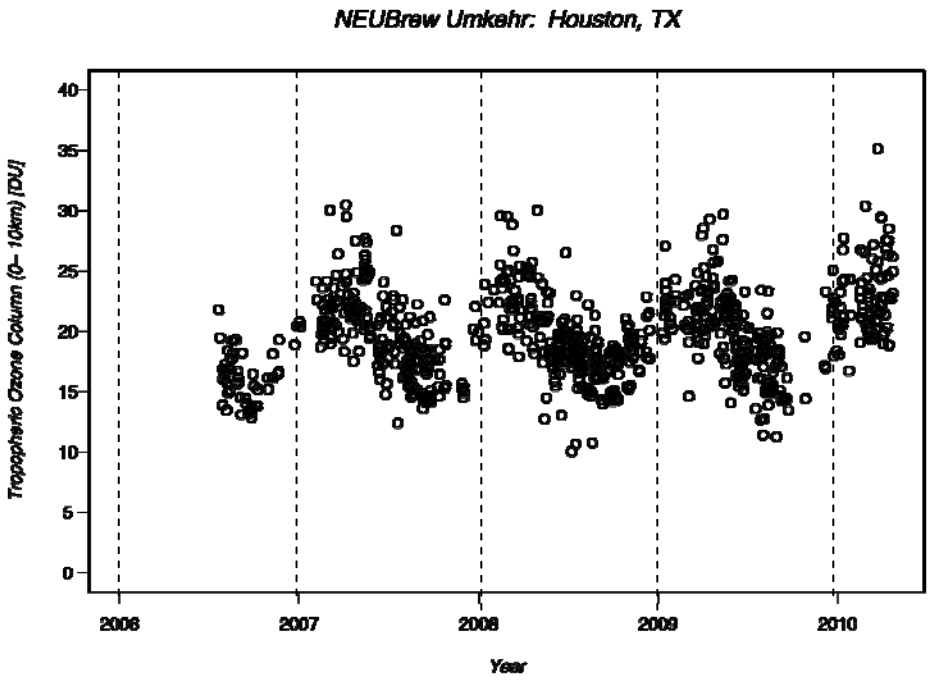

Figure 3.8: NEUBrew tropospheric ozone column amounts (DU) for Houston, TX from August 2006 – present. Daily average tropospheric ozone column amounts are derived from the lowest altitude of the Umkehr Ozone Solution Profile. Peak values occur in early spring while minimum values occur in the fall.

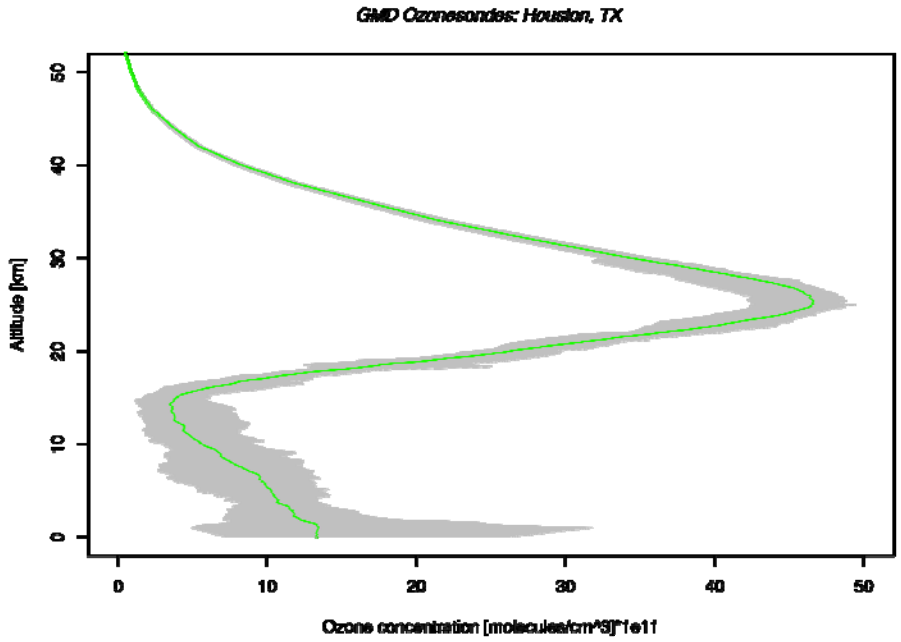

Figure 3.9: GMD Ozonesondes, August 19 – September 14, 2000 (24 profiles). The average profile (green) and maximum-minimum range (grey) as a function of altitude are presented. All 24 observed profiles reached a minimum altitude of 32 km. Profiles were extended from 32 – 72 km using USSA. The average, maximum, and minimum profiles have total ozone values of 308, 356, and 259 DU respectively.

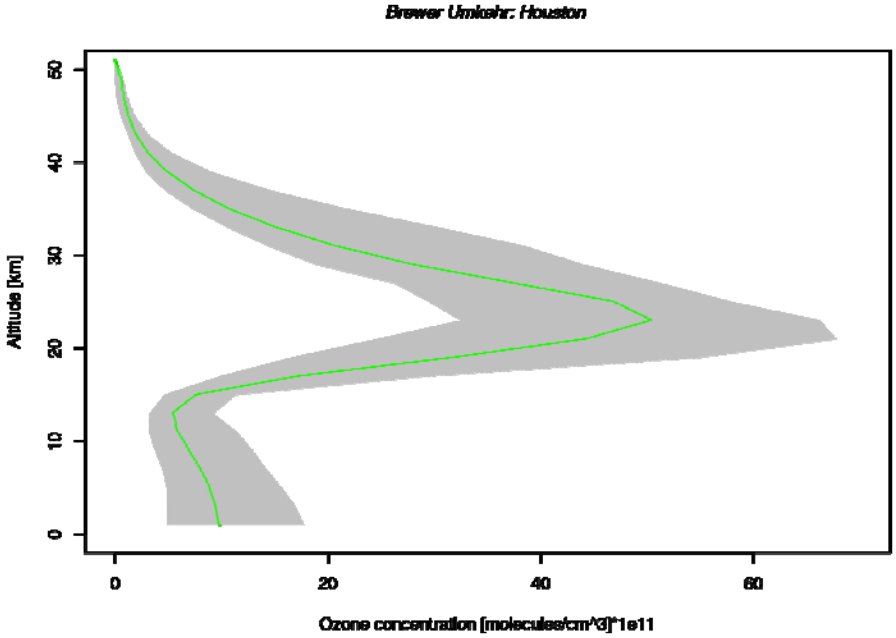

Figure 3.10: INTEX and IONS ozonesondes from Houston, TX. Ozone profiles were filtered to use ozonesondes that reached to 28 km (29 profiles). The average profile (green) and maximum-minimum range (grey) as a function of altitude are presented. Profiles were extended from 28 – 72 km using USSA. The average, maximum, and minimum profiles have total ozone values of 307, 406, and 229 DU respectively.

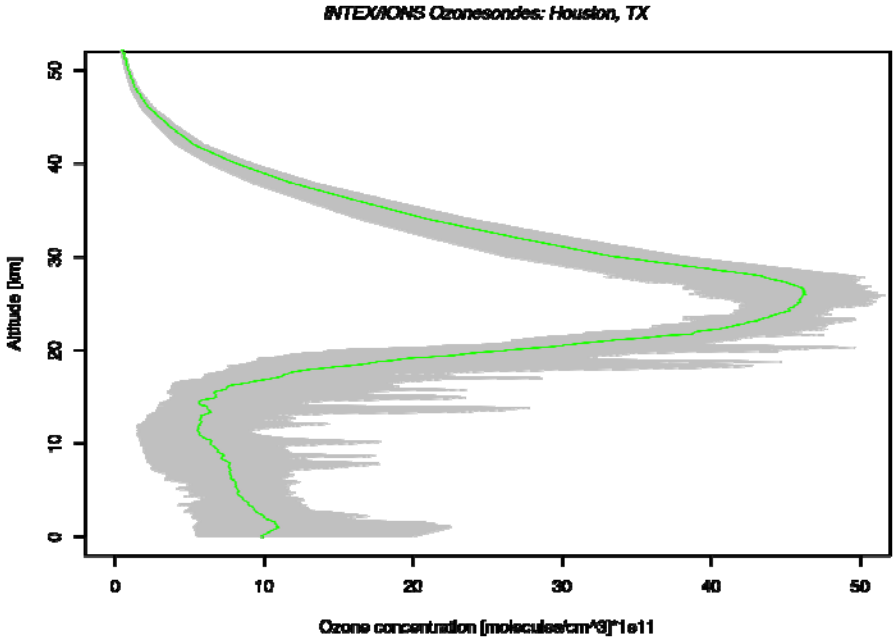

Figure 3.11: NEUBrew Umkehr Ozone profiles for Houston, TX from August 2006 – present (807 profiles). The average profile (green) and maximum-minimum range (grey) as a function of altitude are presented. The average, maximum, and minimum profiles have total ozone values of 283, 444, and 176 DU respectively.

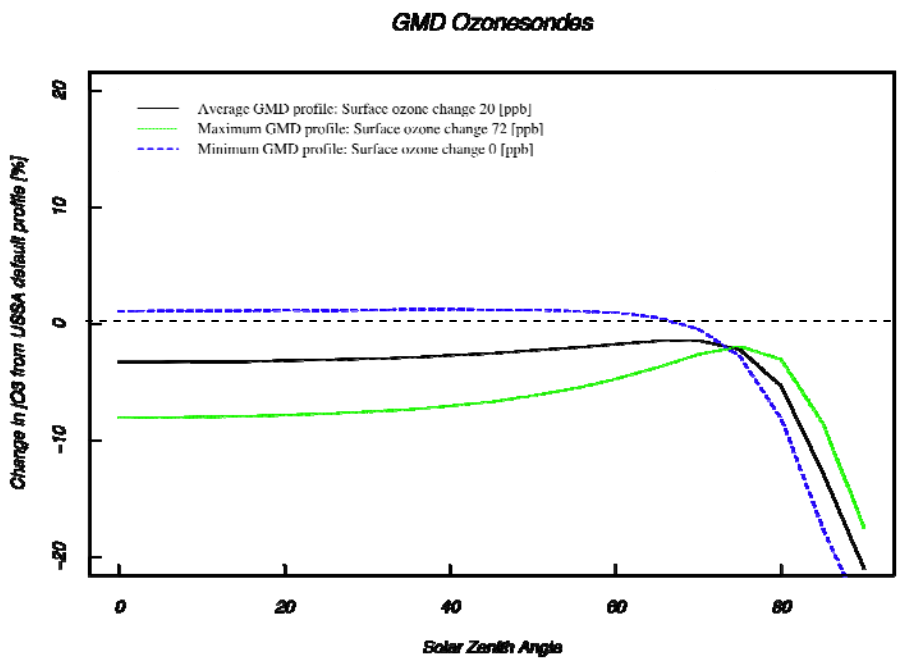

Figure 3.12: Surface $j(O_3)$ using GMD profiles (average, maximum, minimum profiles from 29 profiles) compared to $j(O_3)$ using TUV's USSA ozone profile. The average, maximum, and minimum profiles have total ozone values of 308, 356, and 259 DU respectively, and are compared to TUV's USSA ozone profile normalized to the same total ozone.

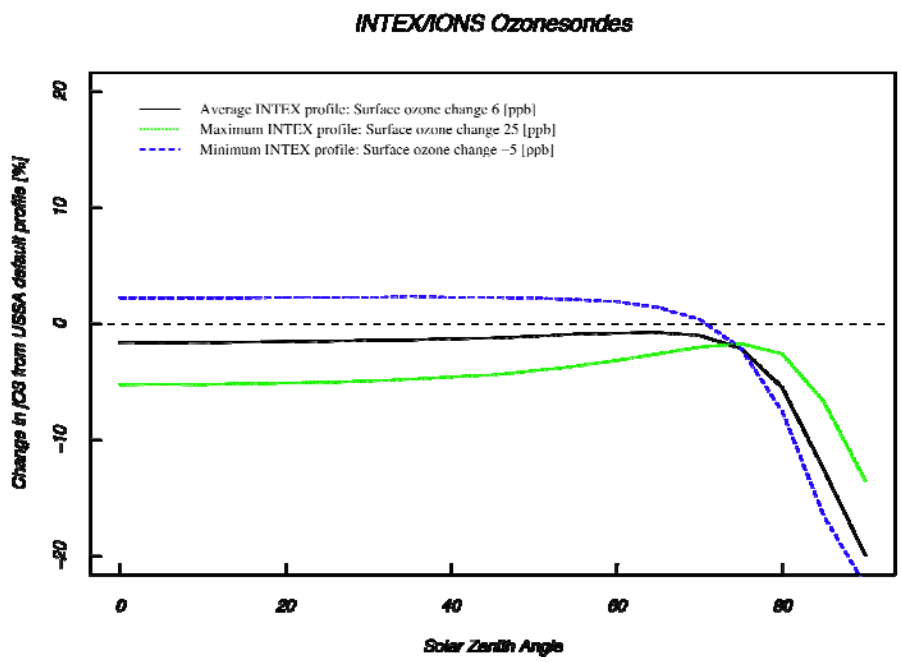

Figure 3.13: Surface $j(O_3)$ using INTEX/IONS profiles (average, maximum, minimum profiles from 29 profiles) compared to $j(O_3)$ using TUV's USSA ozone profile. The average, maximum, and minimum INTEX/IONS profiles have total ozone values of 307, 406, and 229 DU respectively and are compared to TUV's USSA ozone profile normalized to the same total ozone.

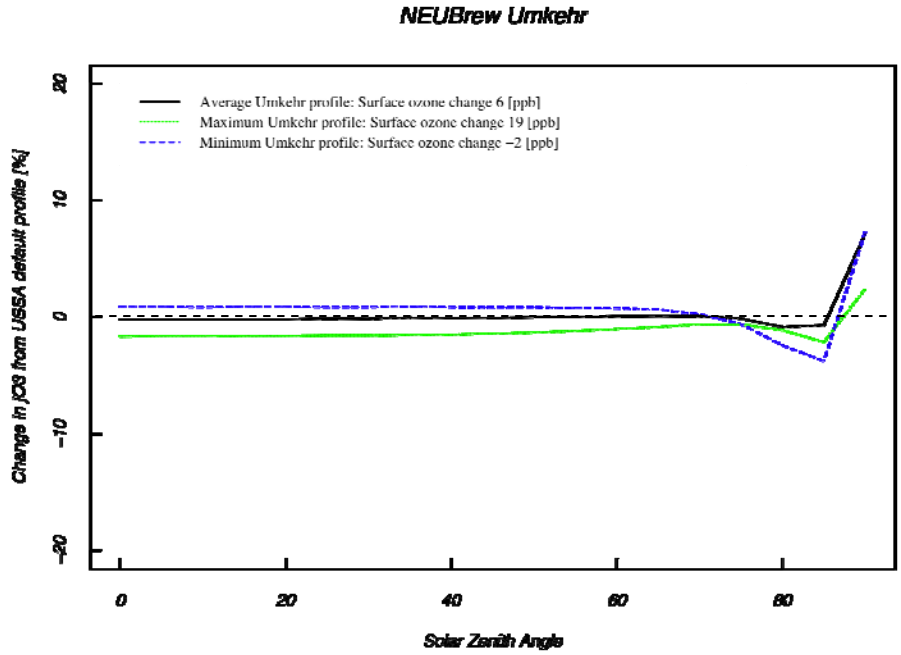

Figure 3.14: Surface $j(O_3)$ using NEUBrew Umkher profiles (average, maximum, minimum profiles from 807 profiles) compared to $j(O_3)$ using TUV's USSA ozone profile. The average, maximum, and minimum profiles have total ozone values of 283, 444, and 176 DU respectively, and are compared to TUV's USSA ozone profile normalized to the same total ozone.

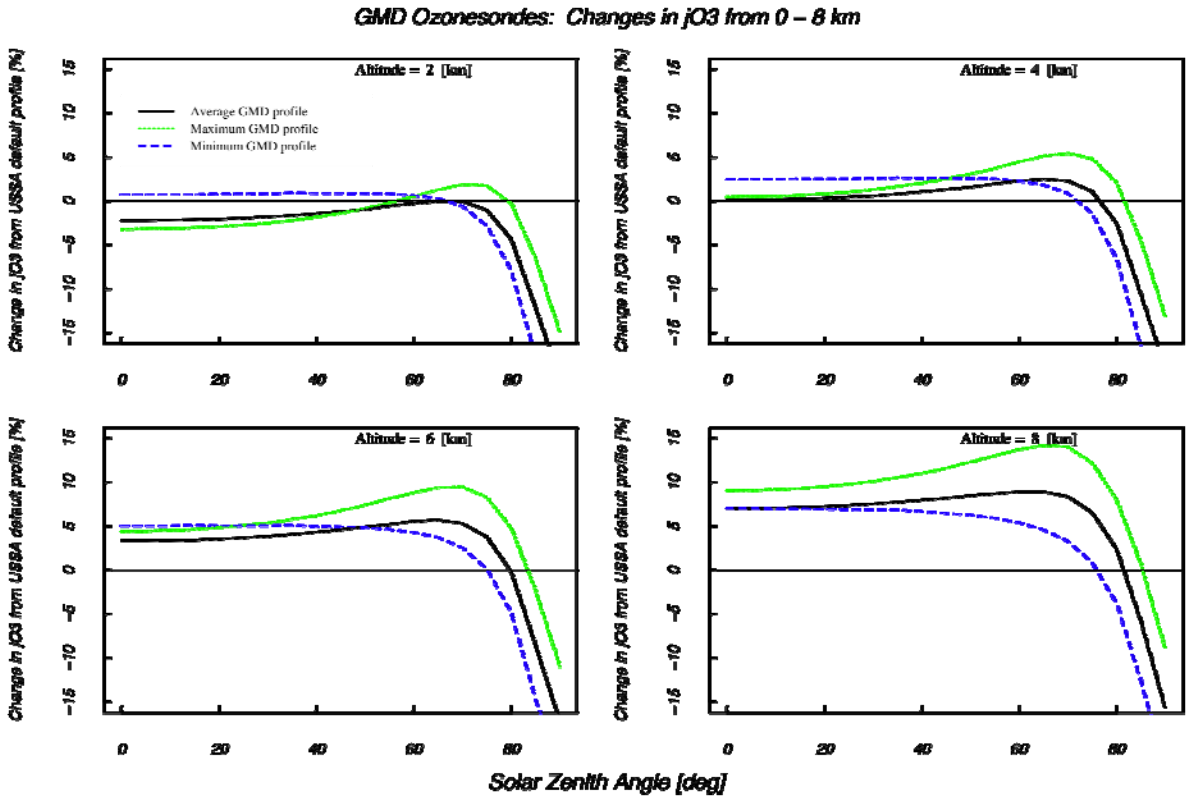

Figure 3.15: Percent changes in $j(O_3)$ when using the default ozone profile versus the measured ozone profiles from GMD ozonesondes at altitude of 2, 4, 8 km.

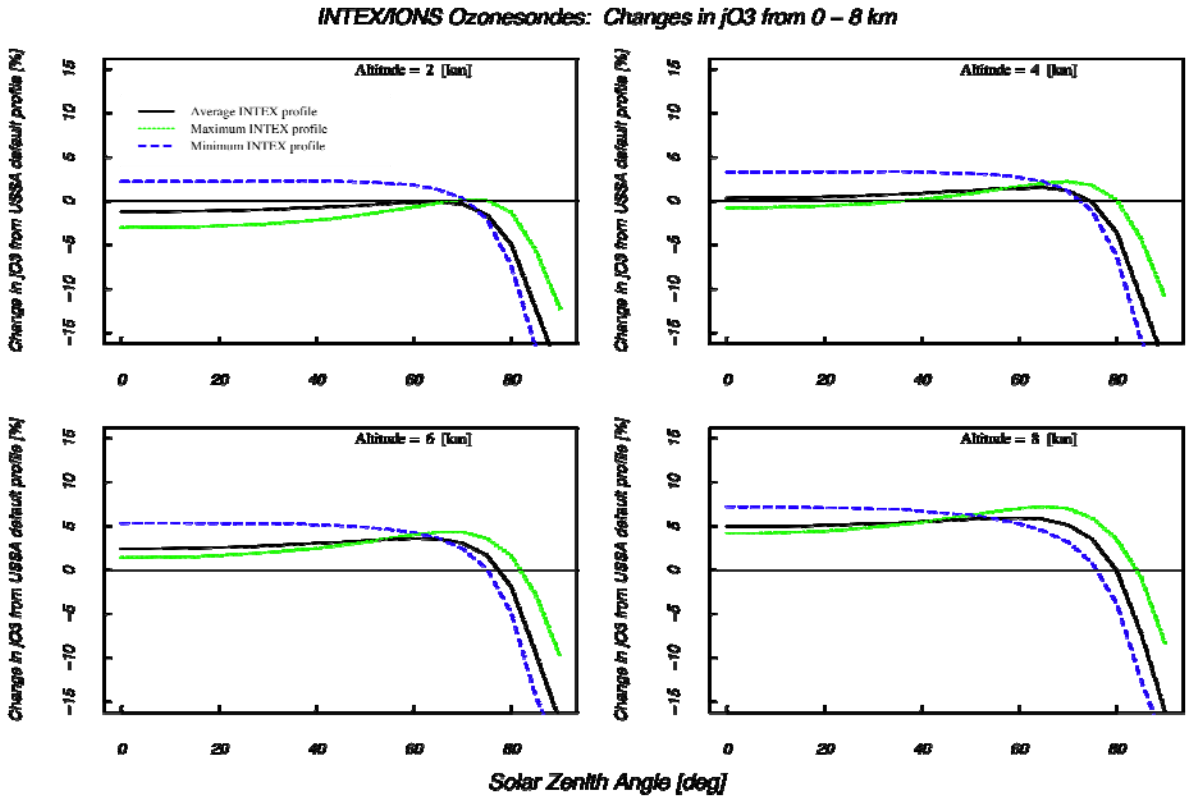

Figure 3.16: Percent changes in $j(O_3)$ when using the default ozone profile versus the measured ozone profiles from INTEX/IONS ozonesondes at altitude of 2, 4, 8 km.

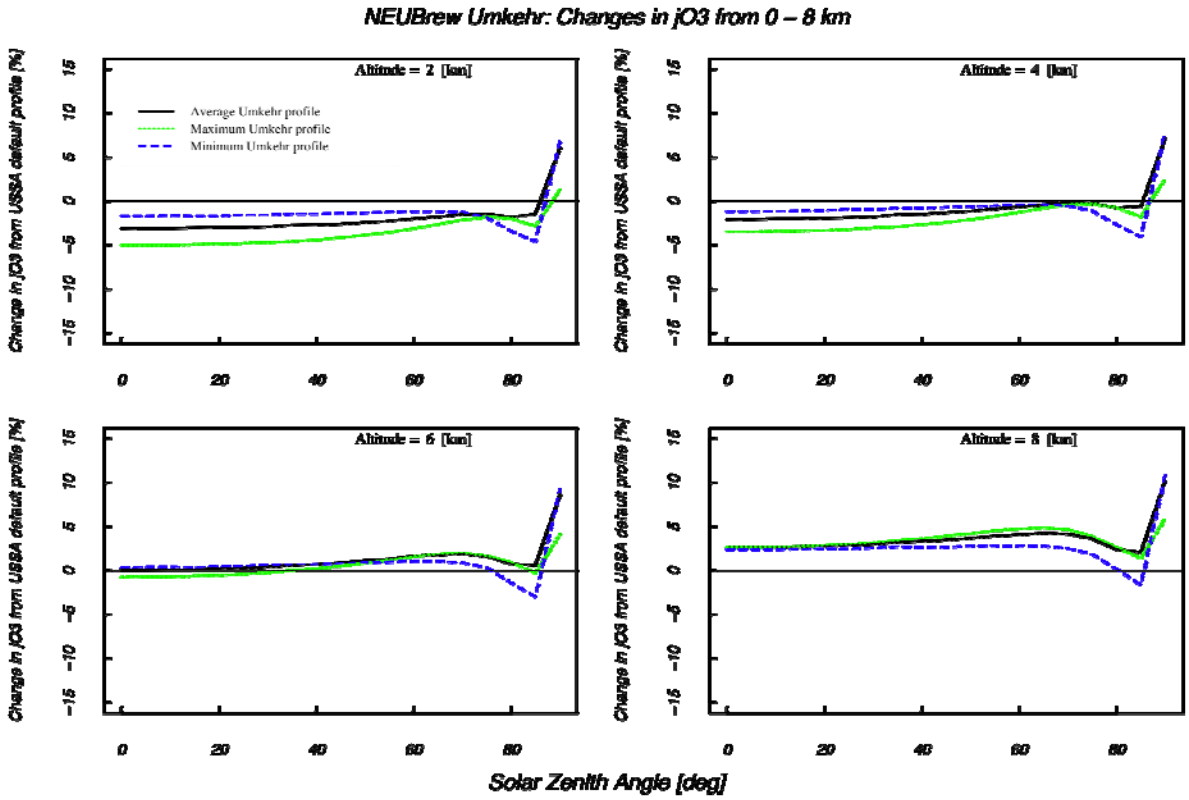

Figure 3.17: Percent changes in $j(O_3)$ when using the default ozone profile versus the measured ozone profiles from NEUBrew Umkehr ozone profiles at altitude of 2, 4, 8 km.

4. Aerosols and UV radiometric quantities

4.1 Sensitivity studies of UV actinic flux and aerosol properties:

Tests were conducted using the TUV radiative transfer model to see how an atmosphere with aerosols differs from one without aerosols and to see what the difference is between scattering aerosols and absorbing aerosols. The default aerosol profile used in the TUV is from Elterman (1966) which has aerosols slowly decreasing from the surface up to 20 km and then decreasing to near zero at 50 km. The use of this profile dictates that aerosols are scattering light well before the lower troposphere is reached. Our literature search has shown that many times the atmosphere is much cleaner at higher levels. Hence, we have developed a second type of profile (modified-tropospheric layer) which is similar to Elterman's from the surface up to 10 km and then decreases to near zero at 15 km and remains so up to 50 km. Figure 4.1 shows the two aerosol extinction profiles. The main purpose of this task is to show how an aerosol profile will affect the UV actinic flux in throughout the troposphere. Figure 4.2 shows the percent change with height of $j(NO_2)$ radiation for an atmosphere using the Elterman profile and scattering aerosols (SSA=0.99) for the sun being directly overhead (sza=0 and at sza = 70). The results for jO_3 will be similar to jNO_2 but will depend on the wavelength dependence of the aerosol properties. Note that an atmosphere with scattering aerosols drastically increases the actinic flux in the troposphere. Figure 4.3 shows the percent change with height of $j(NO_2)$ radiation for an atmosphere using the troposphere layer profile under similar conditions to Figure 4.2. Note how there is less actinic flux in the upper troposphere layer. Figure 4.4 shows the percent change from the Elterman profile to the troposphere layer profile, demonstrating that in the case of a much cleaner stratosphere and upper troposphere that much less actinic flux is present in the upper troposphere layer (at small solar zenith angles) and greater amounts are present near the surface and grows vertically with increasing SZA. Similar tests were conducted for an atmosphere with absorbing aerosols (SSA=0.80) and are given in the quarterly reports.

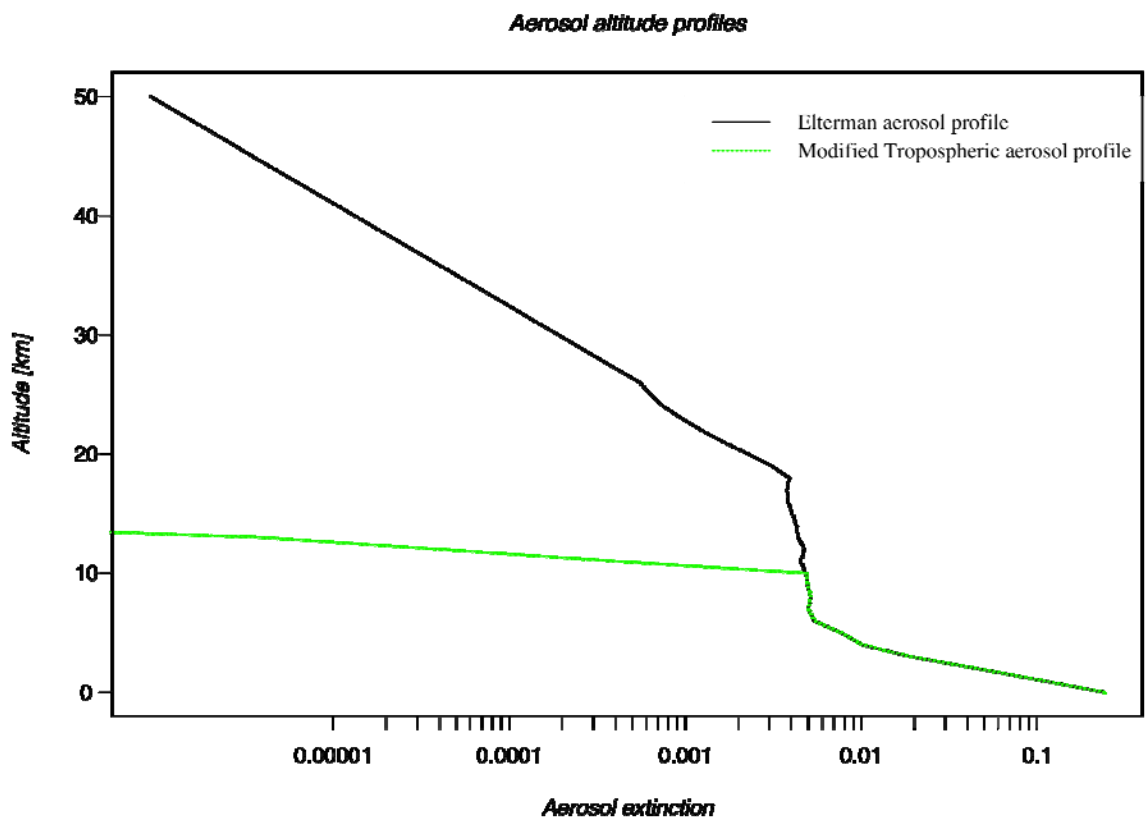

Figure 4.1: Elterman and modified-troposphere aerosol extinction profiles with height [Elterman et al., 1996].

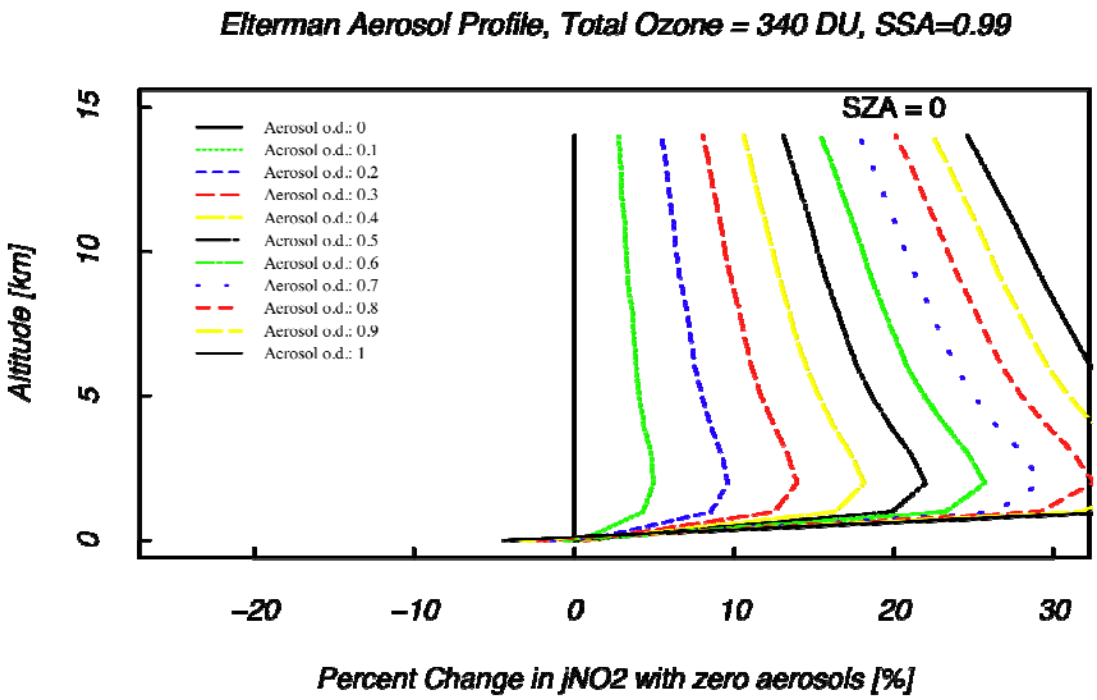

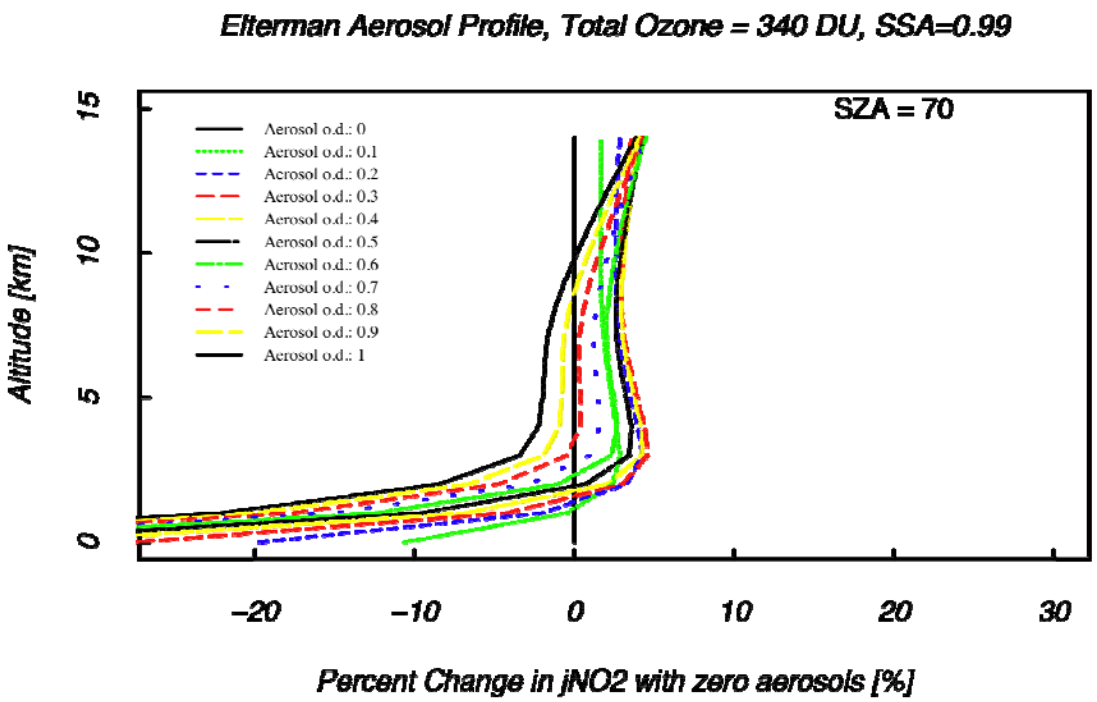

Figure 4.2: Percent change in $j(NO_2)$ for an atmosphere with the Elterman aerosol profile vs one without aerosols for solar zenith angles of 0 (above graph) and 70 (below graph).

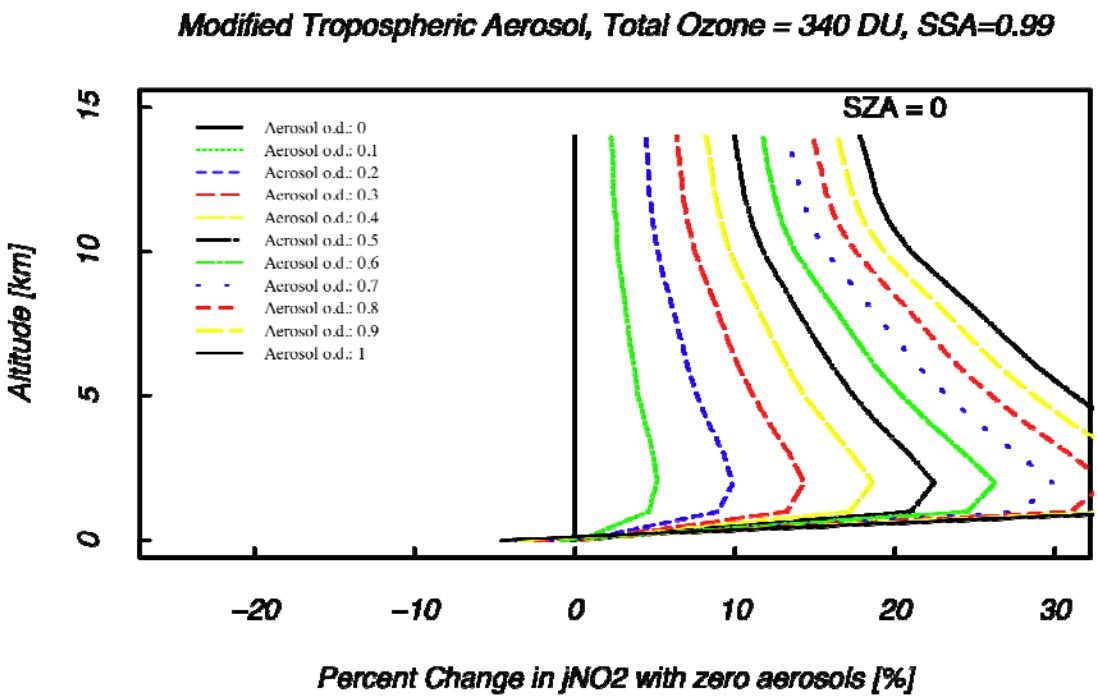

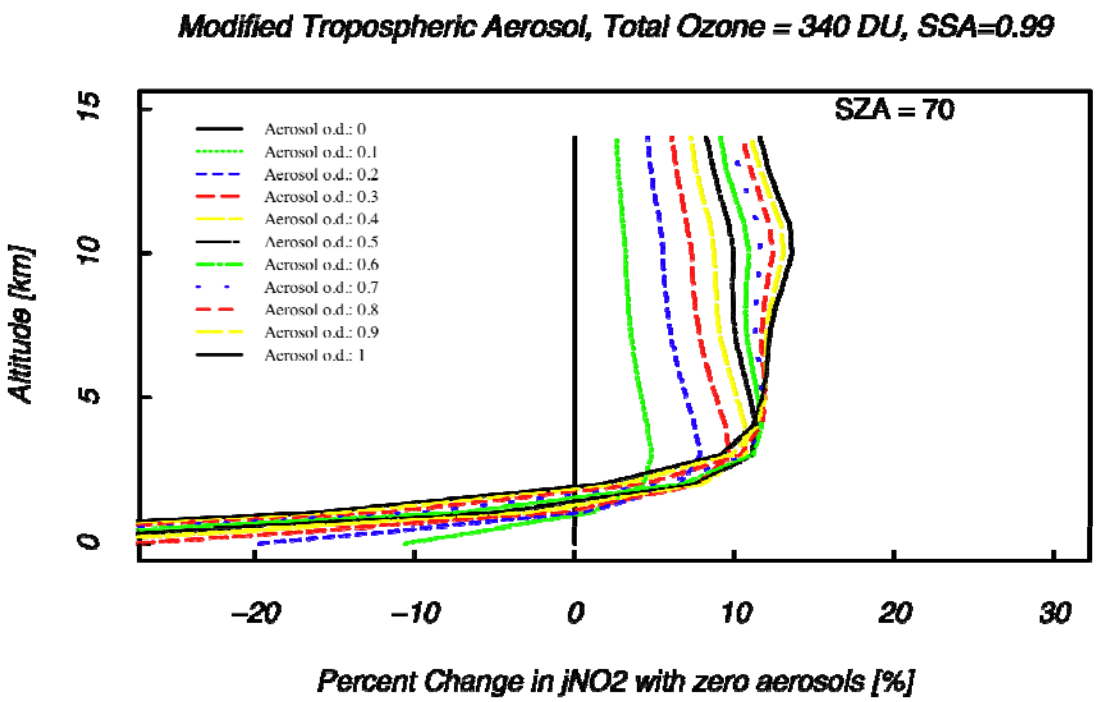

Figure 4.3: Percent change in $j(NO_2)$ for an atmosphere with a modified-troposphere aerosol profile vs one without aerosols for solar zenith angle equal to 0 (above graph) and 70 (below).

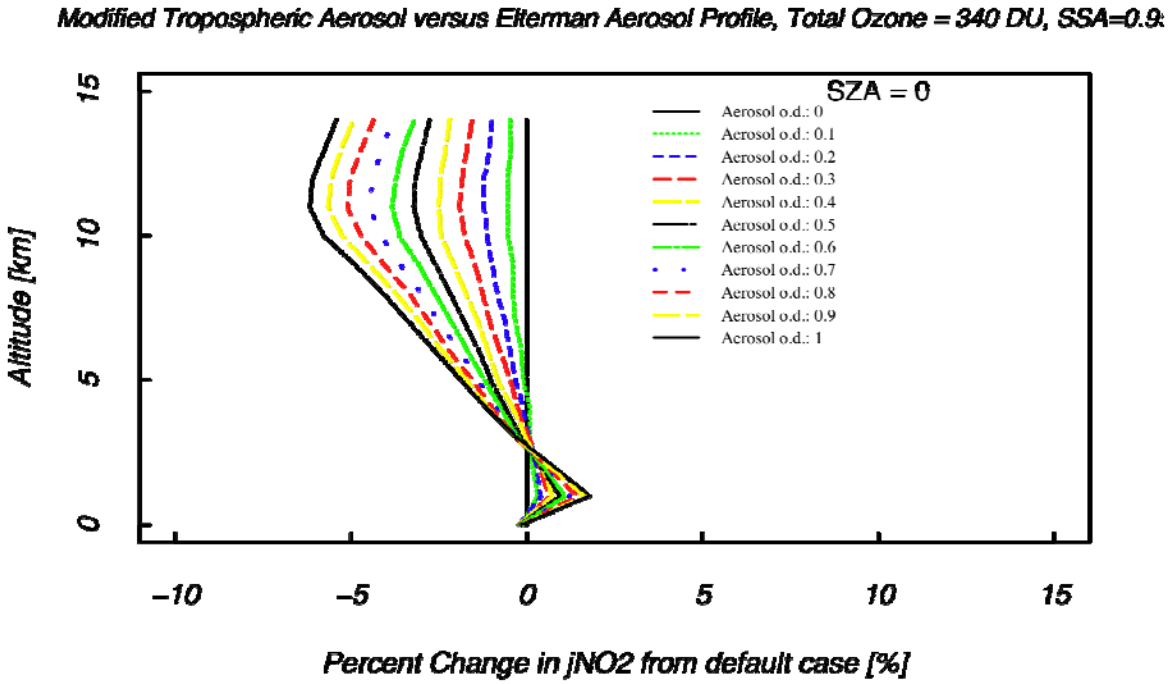

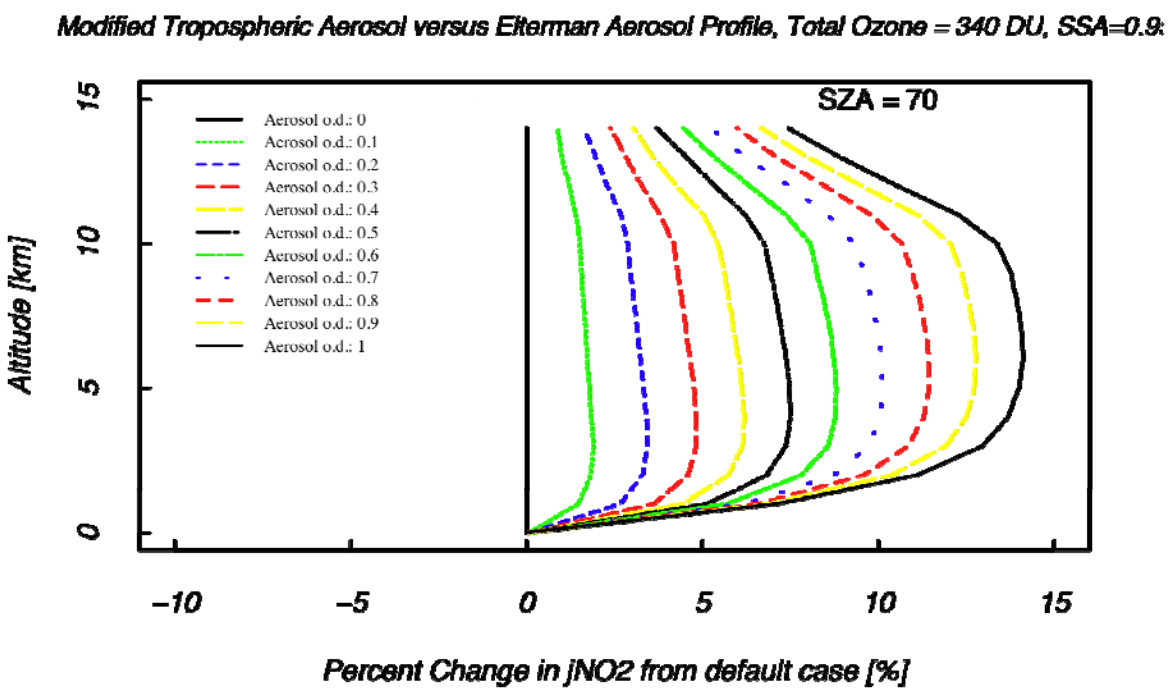

Figure 4.4: Percent change of $j(NO_2)$ between the Elterman profile and modified troposphere aerosol profile at solar zenith angle equal to 0 (above graph) and 70 (below graph).

4.2 Measured Aerosol Optical Depth at Texas Sites

The USDA has an extensive ground network of instruments that measure UV in broad spectral bands and in narrow spectral bands. Their instrumentation includes a Multi-Filter Rotating Shadowband Radiometer (MFRSR) that measures UV and visible light at discrete wavelengths. The instrument has a shadowband that blocks the direct sunlight so a diffuse component can be determined. Observations from this instrument can be used under clear sky conditions to determine aerosol optical depth (AOD) and single scattering albedo (SSA). The SSA is an indicator of the type of aerosols (scattering versus absorbing) in the atmosphere. Currently, a Cloud+AOD product is available from the USDA and a SSA retrieval algorithm has been investigated. We obtained Cloud+AOD observations from the four USDA sites in Texas: Houston, Seguin, Panther Junction, and El Paso, and applied a cloud screening algorithm to retain just the cloud free observations. The cloud screening algorithm was based on the method used in the NOAA/SURFRAD Network [Augustine et al., 2008]. Figures 4.5-4.8 show the daily AOD observations for these four sites for 2007. First order analysis of the figures indicates that Houston and Sequin have considerable greater AOD than Panther Junction and El Paso. There are distinct AOD "episodes" in all four time-series. From Figures 4.5-4.8 thin clouds are not screened adequately suggesting the cloud screening algorithm needs refinement. This in itself would be interesting to delve into, but is beyond the scope of this task.

Utilizing this data we can make better use of our sensitivity studies to gauge the AOD "climatology" around Texas and its impacts on the actinic flux. The SSA data will help us determine the seasonality of absorbing versus scattering aerosols when this becomes available.

4.3 Summary

We performed a literature review of aerosols and photolysis to determine what has been done and what questions still need to be answered. Early scientific questions investigated whether aerosols from industrialized countries may offset potential increases in UV solar radiation due to ozone depletion [Liu et al., 1991; Dickerson et al., 1997; Ma et al., 1997]. Several aerosol studies estimated reductions of 5-18% on UV solar radiation in non-urban areas since the industrial revolution using visibility data [Liu et al., 1991] with combined effects of O_3, SO_2, and aerosols of 9 – 34% on actinic flux [Ma et al., 1997]. Sulfate aerosols were found to enhance photolysis rates by 11-18% under cloud-free conditions [Liao, 1999].

Similar to the sensitivity studies done in the section 4.1, modeling studies were performed using radiative transfer codes and assumed aerosol properties [Dickerson et al., 1997; He et al., 1998; Jacobson, 1997]. For instance sensitivity studies were completed using rural, urban, maritime, and desert profiles [He et al., 1998]. These report similar results to those presented in section 4.1.

There have been a few measurements campaigns of UV and aerosols that have investigated the effects of aerosols on photolysis and subsequent photochemistry. During TEXAQ-II TRAMP, jNO_2 was reduced by 3% due to aerosols during cloud free days [Lefer et al., 2003]. In LA, j-value changes due to aerosols were estimated to decrease near-surface ozone mixing ratios by 5-8% [Jacobson]. During the TRAMP campaign, net ozone production rate was reduced by 8

ppbv/hr due to reductions in photolysis rates [Flynn et al., 2010]. Biomass plumes from Asia were estimated to reduce O_3 by 6 ppbv [Tang et al., 2010].

In summary, aerosols both scatter and absorb UV solar radiation with varying effects on UV solar irradiance and actinic flux in the vertical atmosphere. UV-scattering particles in the boundary layer are found to accelerate photochemical reactions and smog production; while UV-absorbing aerosols such as mineral dust and soot inhibit smog production. Changes in UV on tropospheric ozone production/destruction depends on precursors, e.g. NO_x-rich or poor.

Measurement campaigns to study the effects of aerosols on radiation and photolysis are limited in time and region and questions remain. What are the seasonal distributions and changes in aerosol types and properties in Texas? How do aerosol types and amounts affect photolysis and subsequent tropospheric photochemistry?

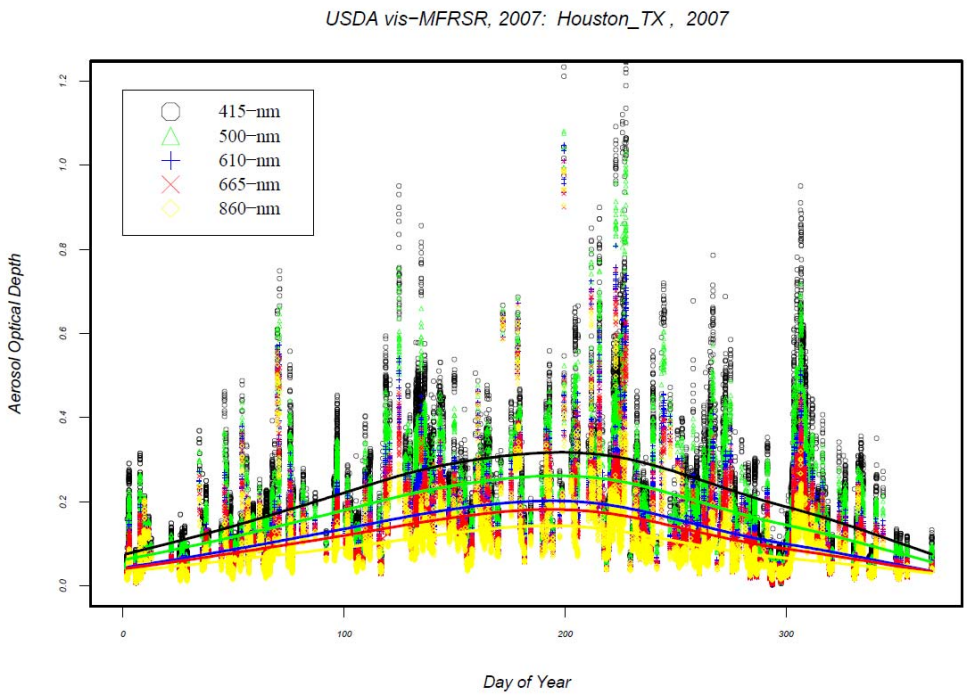

Figure 4.5: Daily MFRSR AOD observations from USDA site at Houston, TX. Low order polynomial for each spectral range are shown as solid lines.

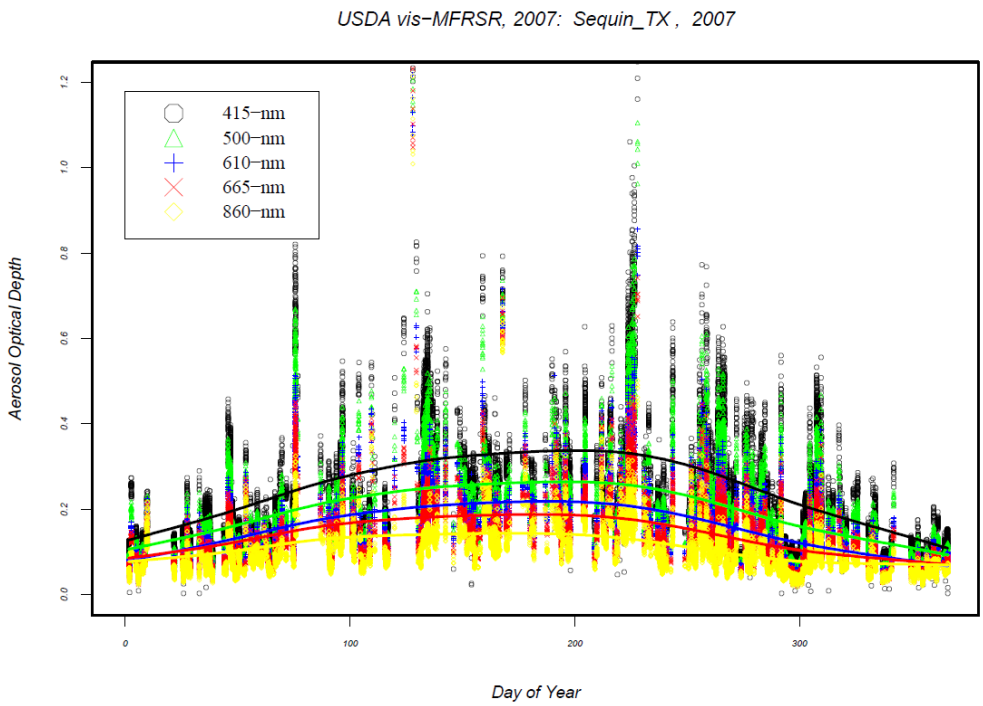

Figure 4.6: Daily MFRSR AOD observations from USDA site at Sequin, TX. Low order polynomial for each spectral range are shown as solid lines.

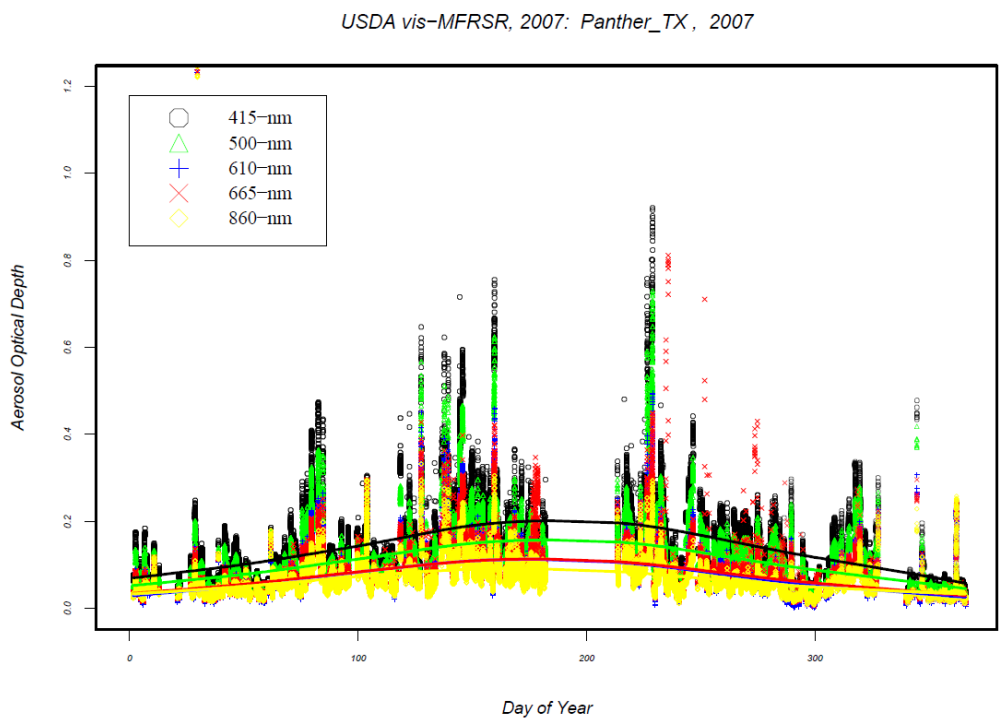

Figue 4.7: Daily MFRSR AOD observations from USDA site at Pather Junction, TX. Low order polynomial for each spectral range are shown as solid lines.

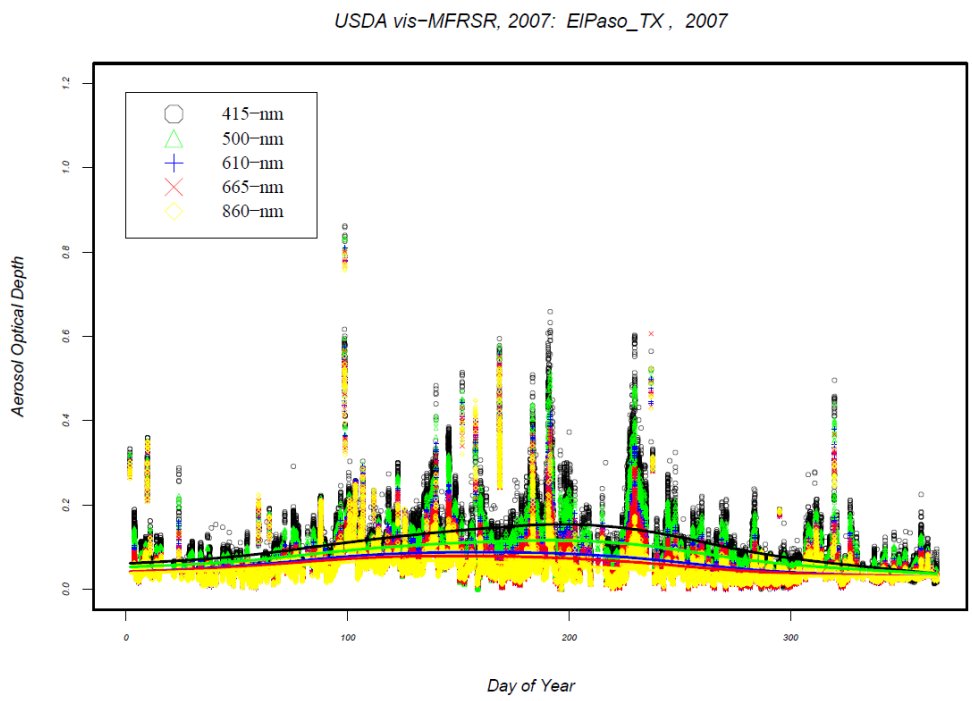

Figue 4.8: Daily MFRSR AOD observations from USDA site at El Paso, TX. Low order polynomial for each spectral range are shown as solid lines.

5. Clouds and UV radiometric quantities

5.1 Introduction

We evaluate the clouds and their role in UV photolysis. First, we use the TUV to evaluate how clouds affect the actinic flux in the troposphere in the presence of aerosols and without. Secondly, we evaluate the accuracy of NWS MOS cloud forecast products.

For this study, we first do a few simple radiative transfer sensitivity studies with cloud and aerosol layers. These are simplistic and do not encompass the complexity of the interaction between aerosols and cloud but give visual magnitude guidelines for simple cases. Next, we acquired NAM and GFS MOS forecasts for several sites in Texas, and compared them with the GFS UV transmission and surface and satellite observations.

We will evaluate two methods of cloud attenuation on UV radiometric quantities. The air quality code uses NCEP NAM and GFS MOS cloud forecast categories (i.e. clear, scattered, broken, and overcast) as surrogates to determine the amount of UV radiation reaching the troposphere layer. MOS cloud probabilities were originally used NCEP's UV Index forecast scheme as cloud forecasts from the NCEP GFS (or AVN as it was called at that time) were inaccurate. However, MOS has characteristics that are detrimental for UV forecasting. For example, MOS will very rarely give a probability of zero or 100 %. Thus using MOS cloud probabilities the UV Index forecasts characteristically over-forecasted the amount of UV radiation reaching the surface

under cloudy conditions and under-forecasted the amount of UV radiation reaching the surface under clear conditions. We have since switched to using the cloud transmission amount directly from the GFS.

5.2 Sensitivity studies of Cloud effects upon actinic flux:

We have modified the TUV to include single and multiple cloud layers. In our experiments, we evaluate the actinic flux change by having placed clouds at 1+2 km (low), 3+4 km (mid), and 6-8 km (high). We also repeated this experiment adding scattering and absorbing aerosols in the lowest kilometer. We modify the optical depth of the clouds for each experiment between 0 and 5, at half unit intervals. Low and middle clouds have been observed to have optical depths up to 5, which are very opaque clouds. High clouds do not get that opaque, so values above 3 should be ignored. Strato-form clouds are assumed for these experiments. Clouds are also assumed to either scatter or transmit radiation (i.e. no absorption).

Figure 5.1 shows that having a cloud placed at 1+2 km increases the actinic flux by up to 40 percent above the cloud due to reflection off the top of the cloud, and decreases the actinic flux below the cloud up to 10 percent. The amount of reflection increases as the solar zenith angle of the sun increases, consequently decreasing the amount transmitted through the cloud.

Figure 5.2 shows that having a cloud placed at 3+4 km increases the actinic flux above the cloud by up to 30 percent, and decreases the actinic flux below the cloud by as much as 10 percent at the surface. Figure 5.3 shows that a cloud placed at 6+8 km increase the actinic flux immediately above the cloud by up to 20 percent for an optical depth of 3.0. Below the cloud the actinic flux is also increased, diminishing as the surface is approached. Both middle and high cloud experiments experience the same affects of increasing the SZA, i.e. greatly decreased actinic flux below the clouds.

Figure 5.4 shows the effects of adding scattering aerosols in the lowest kilometer to the change in actinic flux under high clouds. Little is changed above the lowest kilometer, but the actinic flux is further decreased in the lowest kilometer in the presence of scattering aerosols. Absorbing aerosols further decrease the change in actinic flux near the surface, but only minimally.

We performed one experiment of having multiple layers of clouds at 1+2, 4+5, and 7+8 km. Figure 5.5 shows that actinic fluxes are increased above all three layers of clouds, and is decreased below the lowest clouds. Increasing the SZA reduces the amount of radiation passed through each cloud layer thus decreasing the actinic flux change (not shown).

In summary, due to scattering from the top and within the clouds, the actinic flux above clouds will increase. There is some scattering downward thus increasing the actinic flux immediately below the clouds. The actinic flux is reduced in the lowest kilometer. The amount of scattering below the clouds is reduced as the SZA increases and the decrease in the lowest kilometer is increased. The presence of aerosols in the lowest kilometer has little or no effect above them, but further reduces the actinic flux in the lowest kilometer. Multiple layers of clouds will

increase the actinic flux above and in-between the clouds, but further reduces the actinic flux in the lowest kilometer. The effect of cloud optical depth (COD) on actinic flux and jvalues becomes smaller (smaller percent change per COD) as the COD increases. In the CAMx model, COD less than 5 is treated the same regardless of the value of COD.

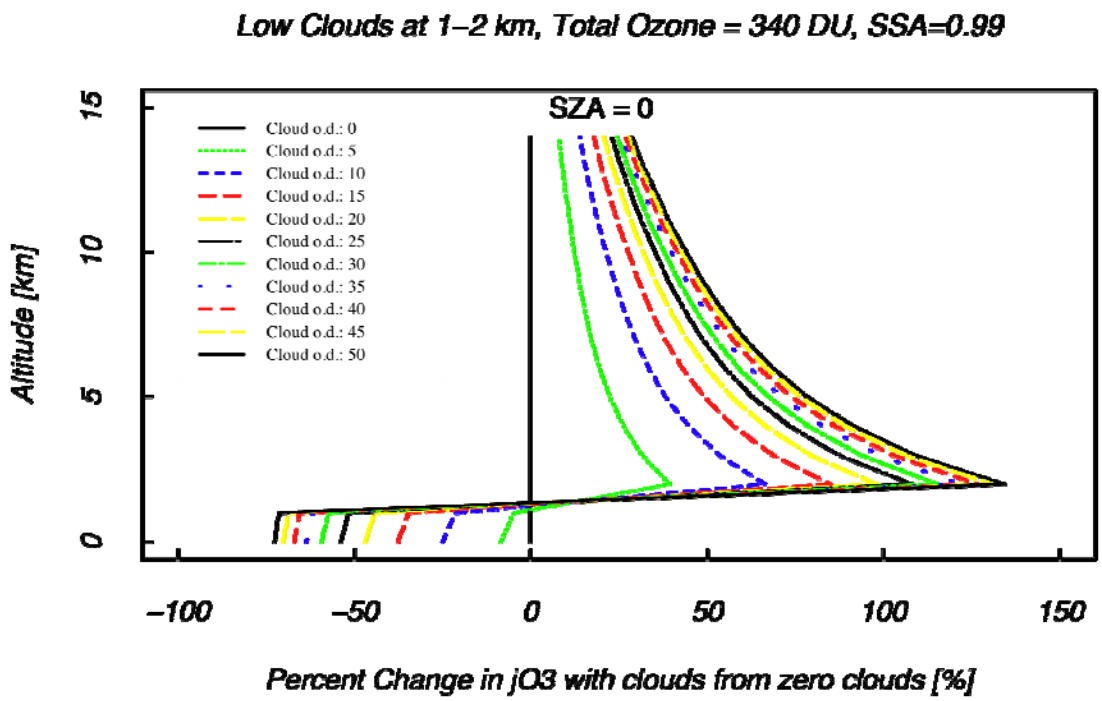

Figure 5.1: Percent increase in actinic flux in the presence of a low cloud of various optical depths with no aerosols in the lowest kilometer.

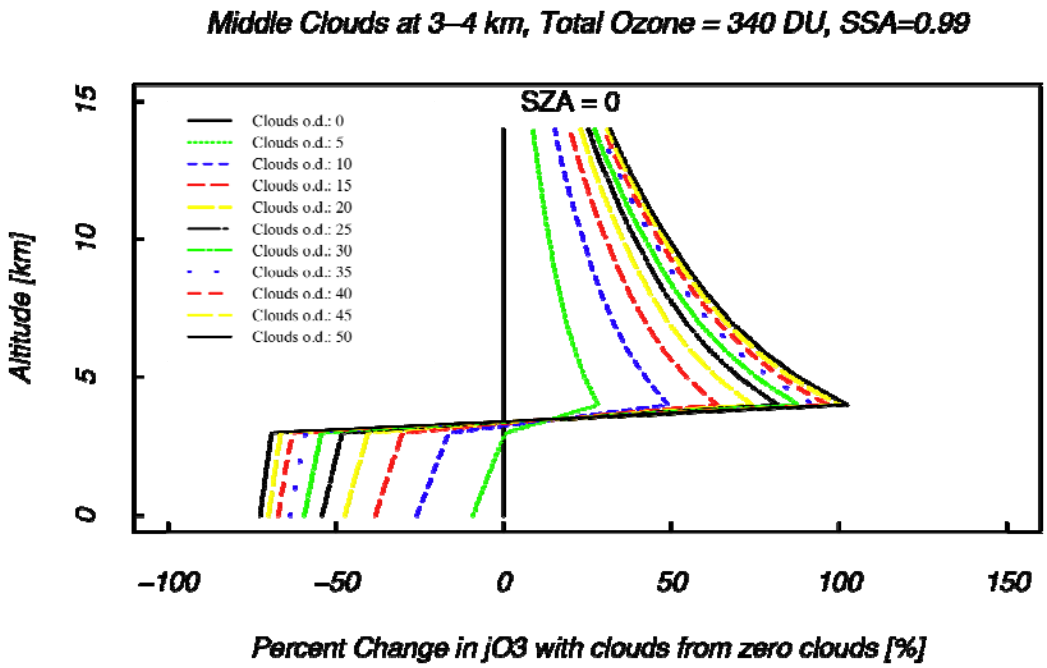

Figure 5.2: Percent increase in jO_3 in the presence of a middle cloud of various optical depths with no aerosols in the lowest kilometer.

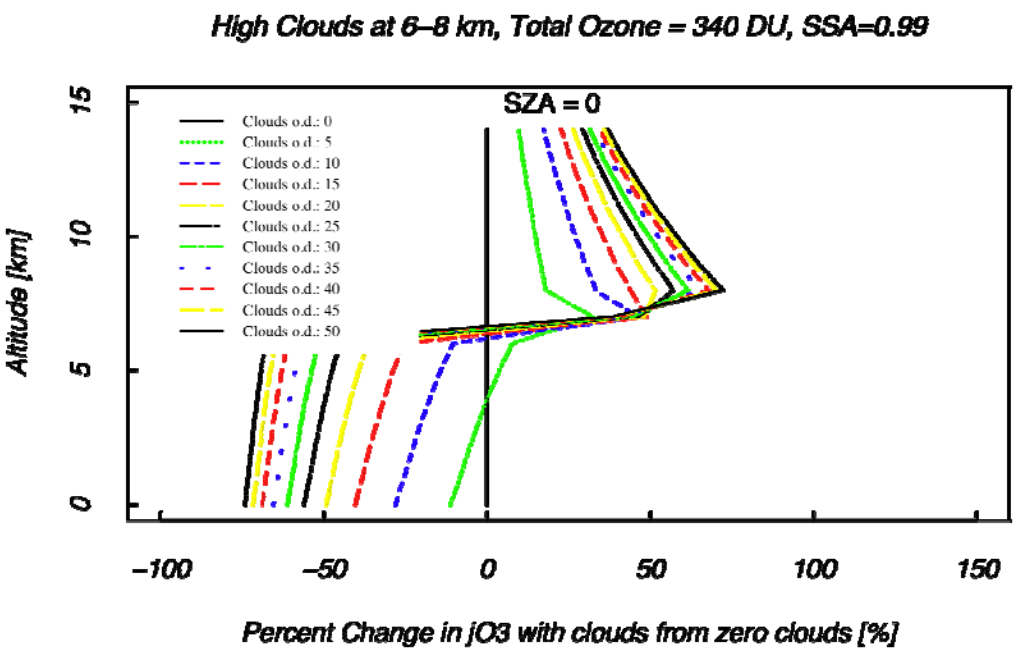

Figure 5.3: Percent increase in jO_3 in the presence of a high cloud of various optical depths with no aerosols in the lowest kilometer.

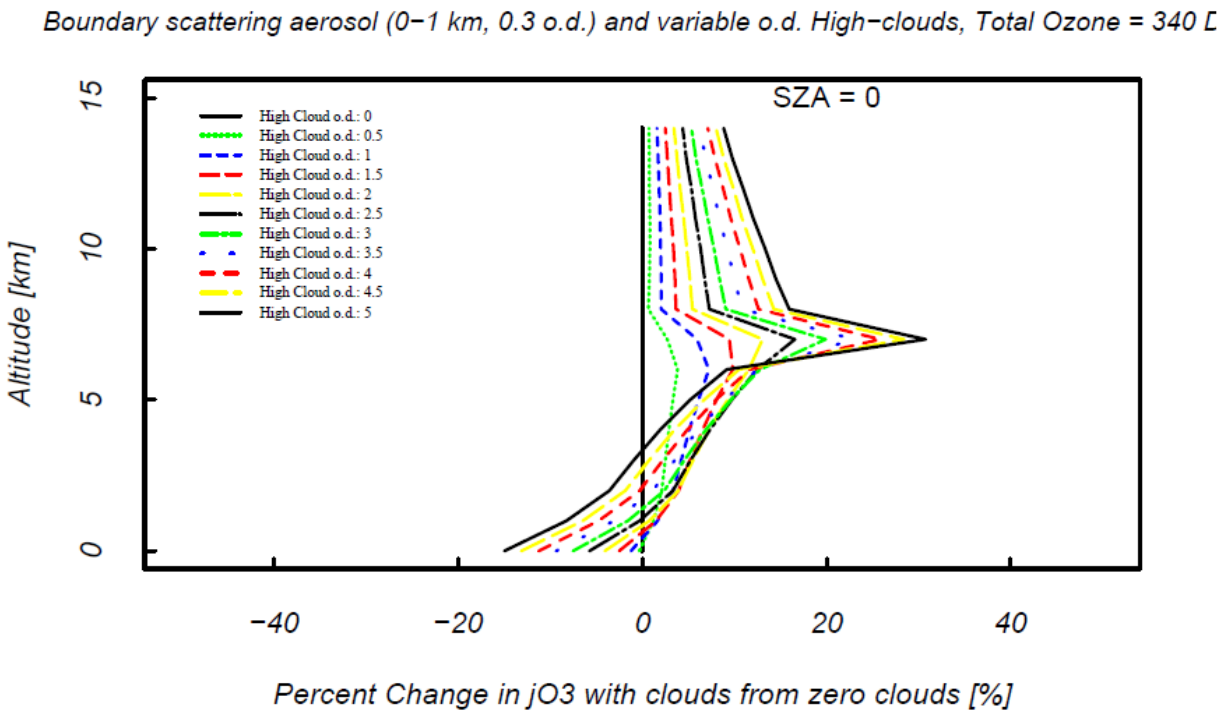

Figure 5.4: Percent increase in jO_3 in the presence of a high cloud of various optical depths with scattering aerosols in the lowest kilometer.

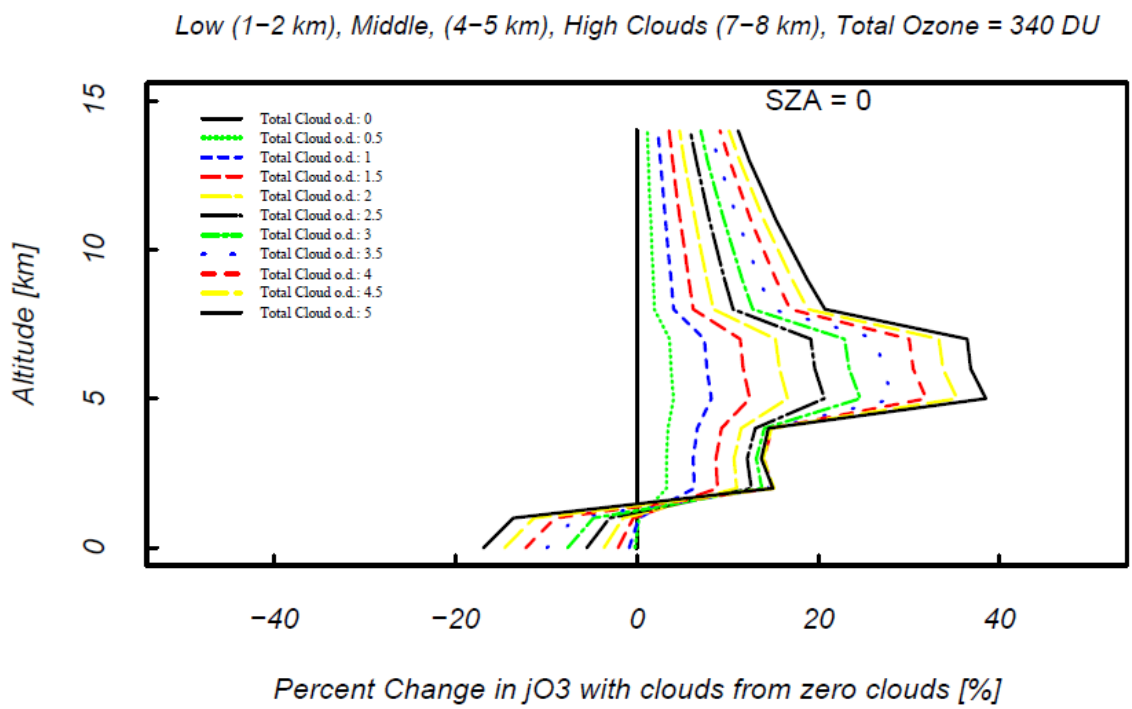

Figue 5.5: Percent increase in jO_3 in the presence of a low, middle, and high cloud of various optical depths with no aerosols in the lowest kilometer for COD 0 - 5. CAMx sets COD < 5 as a special case.

5.3 Cloud forecast evaluation:

5.3.1 Evaluation of GFS and NAM MOS cloud forecasts

The purpose of this part of our project is to see how reliable are the Model Output Statistics cloud forecasts based upon the NCEP Global Forecast System (GFS) model and the North American regional (NAM) model. We use the gridded cloud fraction product from the NOAA/NESDIS GOES Surface and Insolation Product (GSIP) (Laszlo, Tarpley, and Pinker (2002) to validate the GFS and NAM MOS cloud forecasts. We use the 141 MOS stations in Texas as our validation sites. The GSIP is generated from the GOES 13 geostationary satellite (GOES East) imager visible and infrared channels. The imager data is remapped on to a 1/8th degree grid in both latitude and longitude.

MOS forecasts are generated at the 00 and 12 UTC cycle of each model. Using the 00 UTC forecasts a 12 hour forecast will validate at 6 am local standard time (LST) over Texas. Similarly, the 15, 18, 21 and 24 hour forecasts will validate at 9 am, 12, 3, and 6 pm LST over Texas.

The GSIP cloud fraction is available hourly at 45 minutes after the hour. We matched the 1145 UTC analysis with the 12 hr forecast, the 1445, 1745, 2045 and the 2345 UTC analyses with the 15, 18, 21, and 24 hour forecast. We use the average of 37 grid points encompassing the grid point closest to each MOS station location. The 37 grid pattern has a 3,5,7,7,7,5,3 structure. The grid pattern has a radius of about 50 km (or 30 miles) which is similar to the horizon to horizon distance seen from a surface observer.

The GSIP cloud fraction has a range of 0 to 100 percent. The MOS cloud forecast comes in five categories: Clear, Few, Scattered, Broken and Overcast. The range for each category is given in Table 5.1.

Cloud Category	Minimum sky cover (%)	Maximum sky cover (%)
Clear	0	5
Few	6	25
Scattered	26	50
Broken	51	87
Overcast	88	100

Table 5.1: Range of sky cover associated with each cloud category. Taken from the NWS ASOS User's Guide

Figure 5.6 shows the Texas area with the 141 MOS sites marked. These sites are not evenly distributed about the state. Rather they are clustered around Dallas and the eastern side of the state. We did not attempt to thin the MOS sites in order to get a more evenly geographical distribution.

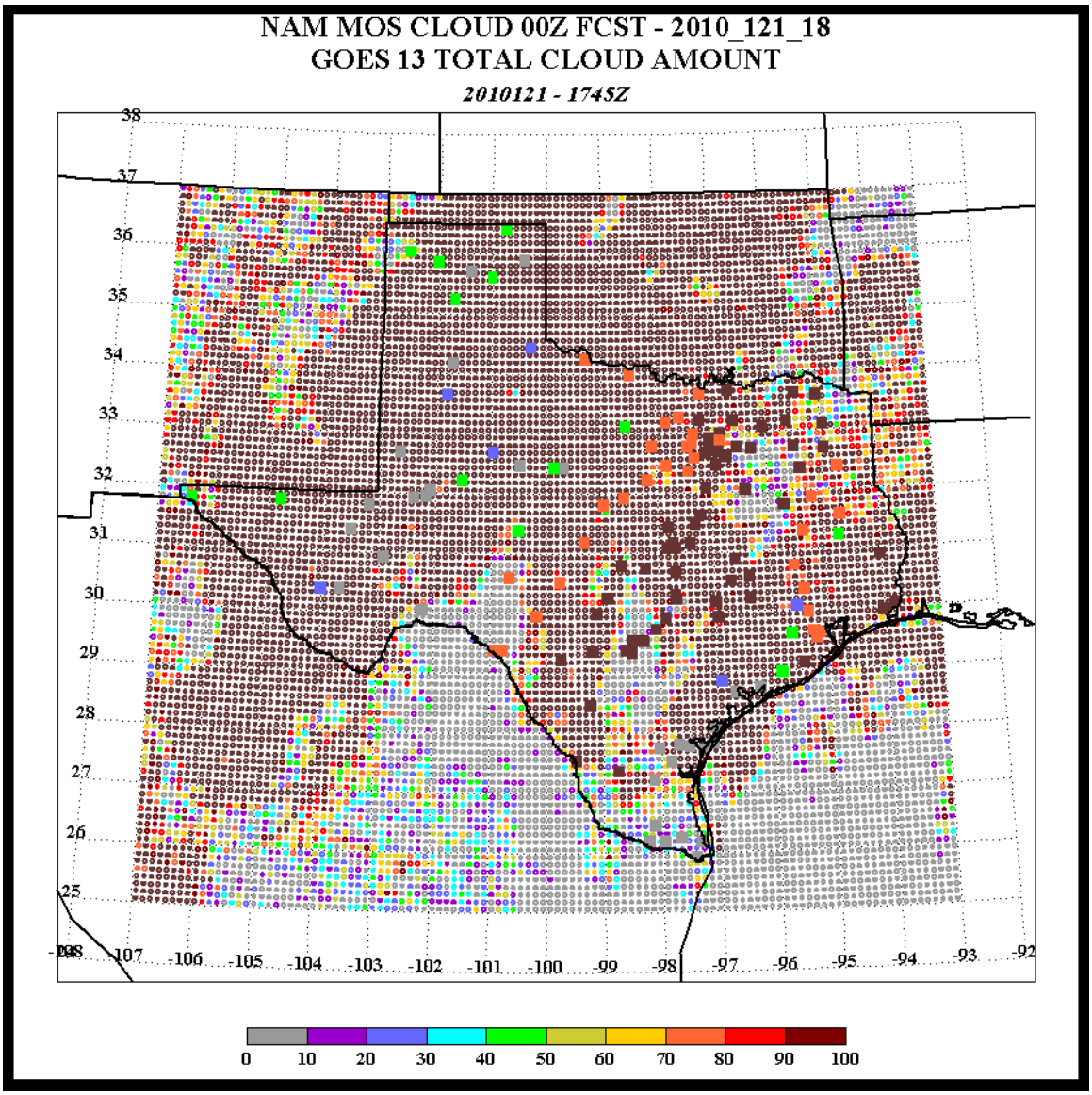

Figure 5.6: Map of Texas and adjoining states with GSIP gridded total cloud fraction observations plotted as color diamonds at their grid location for May 1, 2010 at 17:45Z. The diamonds are colored using the shown color coding to reflect the percent cloud cover. Also plotted are the 141 MOS forecast sites in Texas also color coded to reflect the MOS cloud forecast amount for this same time period.

Figure 5.6 also shows the GSIP total cloud amount for the gridded area encompassing Texas (latitude range: 25N-37N, longitude range: 93W-107W). Each $1/8^{th}$ x $1/8^{th}$ degree cell is color coded to reflect its total cloud amount. The MOS sites are also colored using the same color scale to reflect the NAM MOS cloud amount for the matching time period. Where the colors of

the MOS stations and the GSIP grid are the same then there is good forecast. Figure 5.7 shows the actual GOES 13 (East) visible band image this same day and time. One can compare the GSIP total cloud amount with the image to see how well the GSIP algorithm captures the correct total cloud amount.

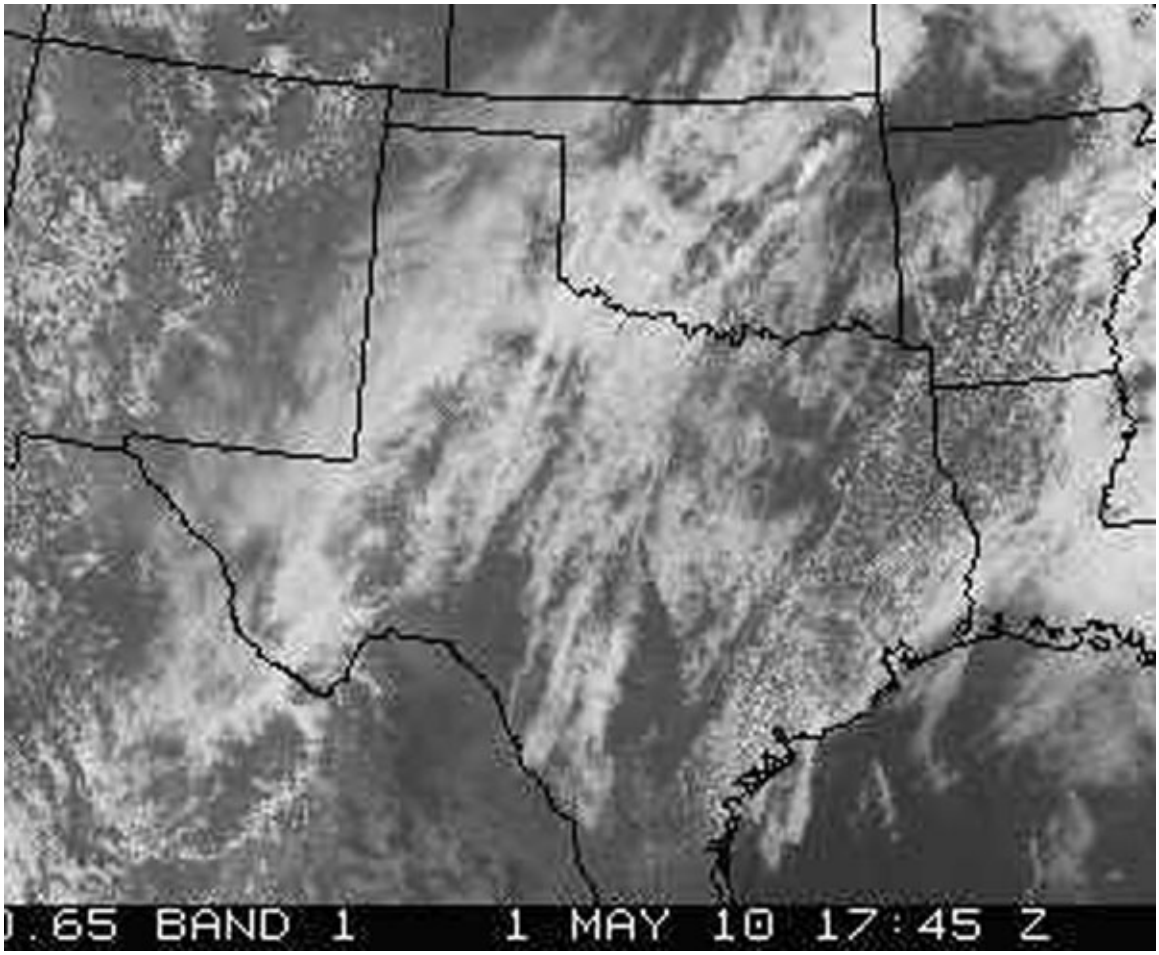

Figure 5.7: GOES 13 (East) visible (650 nm) band image for May 1, 2010 taken at 17:45Z.

5.3.1.1 Results

For each day between May 1 and June 30, 2010, match-ups were made for the GFS and NAM MOS forecasts at 15, 18, 21, and 00Z (9, 12, 15, 18 Local Standard Time) generated at the 00Z cycle. GSIP total cloud amounts used were the 14:45, 17:45, 20:45, and the 23:45Z products. The GFS and NAM MOS forecasts were separated into their five cloud categories: clear, few, scattered, broken, and overcast. The GSIP average cloud amount for the MOS sites in each of these categories were then binned into the same categories using the ASOS cloud amount guidelines. Figure 5.8 show what percentage of the GSIP observations were in each NAM MOS cloud categories for each forecast period (the GFS results are very similar). Figure 5.8 shows that 30-60 percent of the GSIP "clear" cloud observation occurred when the NAM MOS "clear" forecast was made. Consistently, 20 percent of the "clear" observations occurred when NAM

MOS made a "few" forecast. Fewer percentages occurred when "scattered", "broken" and "overcast" forecasts were made.

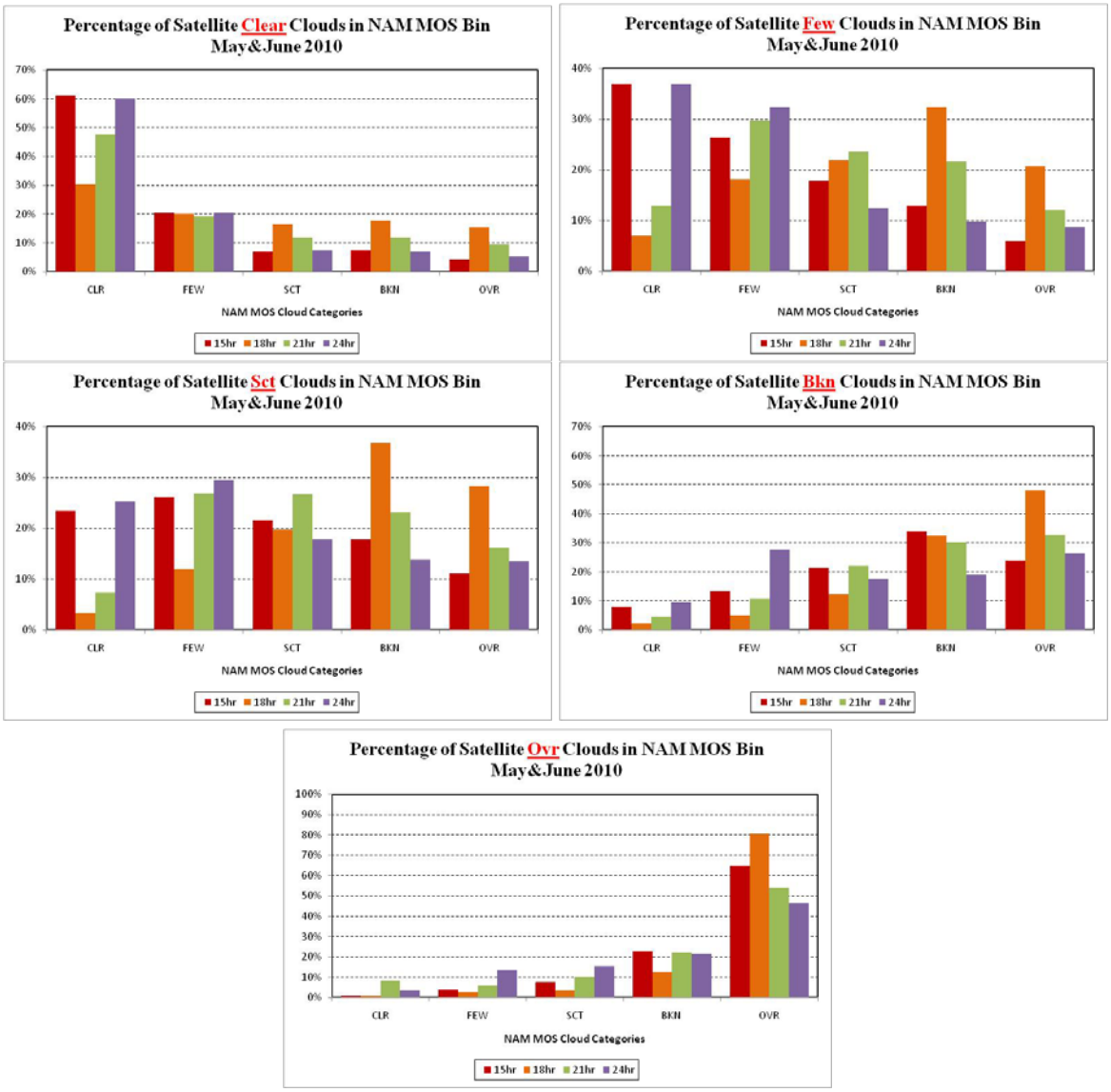

Figure 5.8: Summaries of the percentage of satellite observed "clear"(a), "few"(b), "scattered"(c), "broken"(d), and "overcast"(e) cloud amounts binned into the MOS cloud amounts for the 15, 18, 21 and 24 hour (9, 12, 15, and 18 LST) forecasts.

GSIP observations in the "few" cloud amounts occurred mostly when the NAM MOS forecast was "clear" or "few" for the 15 and 24 hr forecast, but less "clear" and more evenly distributed between the other four categories for the 18 and 21 hr forecast.

GSIP observations in the "scattered" cloud amounts occurred mostly in the "clear", "few", and "scattered" cloud amounts for the 15 and 24 hr forecast, but much less "clear" and more evenly distributed between the other four categories for the 18 and 21 hr forecast.

GSIP observations in the "broken" cloud amounts occurred mostly in the "broken" and "overcast" cloud amounts for all four forecast times and much less so in the "clear" and "few" cloud forecasts.

GSIP observations in the "overcast" cloud amounts occurred predominantly when "overcast" cloud forecasts were made for all four forecast times.

5.3.1.2 Summary

- When GFS and NAM MOS produce a "clear" or "overcast" forecast, the satellite observations tend to agree.
- When GFS and NAM MOS produce a "few" or "scattered" forecast, the satellite observations indicate that most any cloud amount may occur.
- When GFS and NAM MOS produce a "broken" forecast, the satellite observations indicate that either "broken" or "overcast" conditions will occur.

5.3.2 Diurnal patterns:

The GFS and NAM MOS cloud forecasts and the GSIP cloud observations were examined to see if there was similarity in their diurnal characteristics. Figure 5.8 shows the percentage of the forecasts and observations in each cloud category at 6, 9, 12, 15 and 18 LST. There is a predominant preference for the NAM MOS to make a "clear" or "overcast" forecast at both 6 and 9 LST. The GFS MOS forecasts predominantly "clear" 6, 9, and 18 LST. "Overcast" cloud forecasts are only dominant at 6 LST and are less dominant at the other hours than the NAM forecasts. The GSIP cloud observations at 6 LST are too biased by the large sun angle to produce an accurate cloud amount. At the other times, the "overcast" cloud category is dominant at the 9, 12, and 15 LST. The "clear" category occurs least at 12 LST, but increases towards the morning and evening hours.

5.3.2.1 Summary

The diurnal GFS and NAM MOS cloud forecast preference is different than that of the GSIP observations. The satellite observes the "overcast" conditions to dominate at 12 LST, with very few "clear" observations at that time. However, the preferred time for the GFS and NAM MOS "overcast" cloud forecast is at 6 LST. The NAM MOS "overcast" cloud forecast is also preferred at 9 LST. "Clear" cloud forecasts occur next in preference at both 6 and 9 LST. At the other times of the day there is no preferred forecast cloud amount.

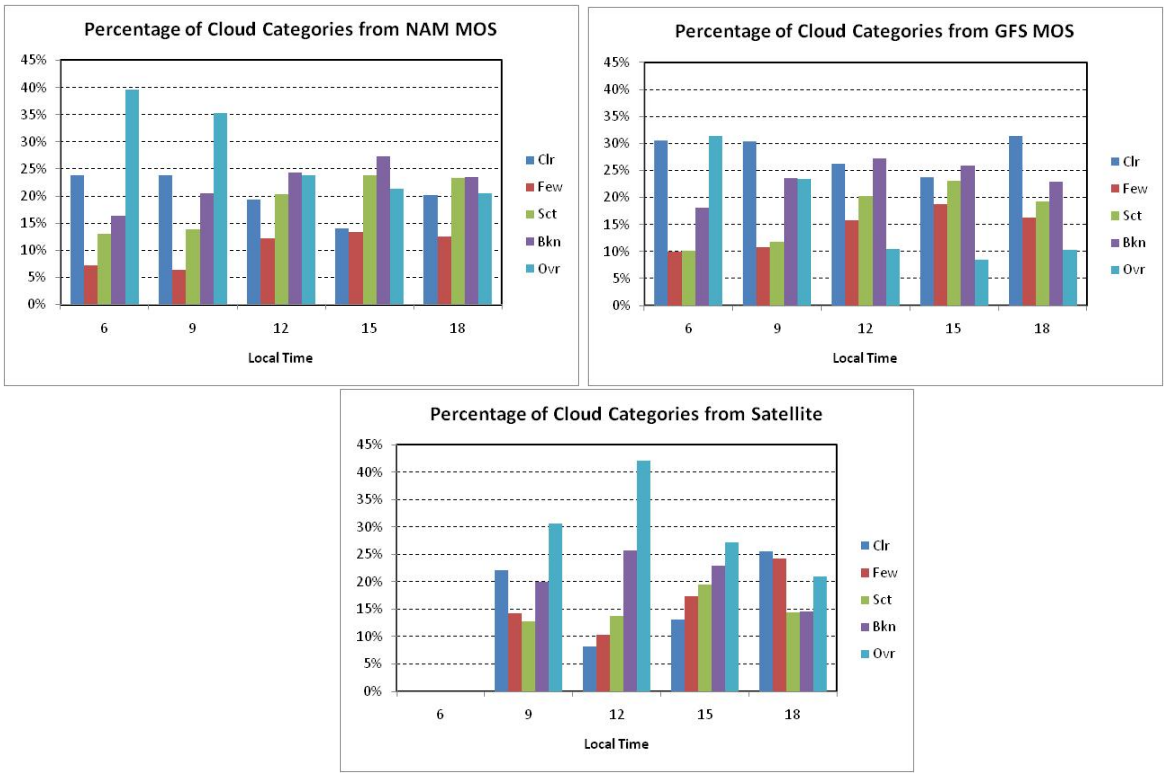

Figure 5.9: Diurnal characteristics of the NAM MOS (a) and GFS MOS (b) cloud forecasts, and GSIP (c) cloud observations.

5.3.3 Section Summary:

The purpose of this comparison was to determine the accuracy of the GFS and NAM MOS cloud forecasts. Cloud fraction amounts from the GOES imager was used to validate the forecasts. In the early morning and evening, when the MOS forecasted "clear" sky conditions, those conditions were observed to occur 60 percent of the time. Including cloud observations in the "few" category increases the observations to 80% of the time. Conversely, MOS forecasts of "overcast" cloud conditions are observed to occur 50-70% of the time. Including "broken" cloud observations increases the occurrence to nearly 90% of the time. Forecasts of the other three categories have much lower accuracy. This is important for air quality forecasts as we have shown that clouds can greatly attenuate the actinic flux. An error in a cloud forecast can produce equally large errors in the forecast amount of ozone production. Apparently, the "clear" and "overcast" cloud amount categories are forecasted well. However, confidence in the cloud forecast is much less for the other categories as then will be the ozone production forecast.

6. Conclusions

Very few previous studies have evaluated the effect of changes in the ozone profile on actinic flux or photolysis rate constants. Few of the studies have been done within the U.S. The work here uses ozone profiles specifically from Texas and compares to the standard profile used in the TUV Radiative Transfer Model and the CAMx model.

The effect of changes in the ozone profile from the standard ozone profile has very little effect on $j(NO_2)$ of less than 0.5%. Larger effects are seen in shorter wavelengths of actinic flux and in $j(O_3)$. Changes in $j(O_3)$ will affect the concentration of the hydroxyl radical in the atmosphere and therefore the oxidative capacity of the atmosphere. Evaluating changes in the hydroxyl radical and its effect on tropospheric ozone concentrations was outside the scope of this investigation.

Sensitivity tests showed that usage of the standard ozone profile in computations of ozone photolysis rate constants will slightly underestimate by 1-2% the photolysis rate constants for small surface ozone amounts and will overestimate the surface photolysis rate constants by 2-8% for larger amounts of surface ozone. Another sensitivity test showed that if the ozone peak is higher than the standard profile's by 2 to 6 km, there is a 1-2% increase in the ozone photolysis rate constant.

In practice, the USSA standard ozone profile is equally adjusted to match the forecast total column ozone amount. This adjustment process over-adjusts the surface ozone amount. We found through comparisons with multiple ozonesonde campaigns that doing so results in producing incorrect photolysis rate constants at the surface. We found that when ozonesonde profiles had smaller (larger) surface ozone amounts than the adjusted USSA standard ozone profiles; the ozone photolysis rate constant at the surface also was smaller (larger). The ozone photolysis rate constant percent change also seems to be a function of the percent change of the surface ozone amount. We also found that because the ozonepause of the USSA standard profile is near 10 km, while the ozonepause for all three campaigns averaged near 15 km, the ozone photolysis rate constants at different altitudes for the ozonesondes from the three campaigns were greater than that determined from the adjusted standard profile.

Aerosols both scatter and absorb UV solar radiation with varying effects on UV solar irradiance and actinic flux in the vertical atmosphere. UV-scattering particles in the boundary layer are found to accelerate photochemical reactions and smog production; while UV-absorbing aerosols such as mineral dust and soot inhibit smog production. Consequently, this will either enhance $j(NO_2)$ and $j(O_3)$ photolysis rates or decrease them. A literature review of aerosols and photolysis revealed that scattering sulfate aerosols were found to enhance photolysis rates by 11-18% under cloud-free conditions [Liao, 1999]. On the other hand, during the TRAMP campaign which studied absorbing aerosols, the net ozone production rate was reduced by 8 ppbv/hr due to reductions in photolysis rates [Flynn et al., 2010].

Questions that remain pertinent to this study are: What are the seasonal distributions and changes in aerosol types and properties in Texas? How do aerosol types and amounts affect photolysis and subsequent tropospheric photochemistry?

The actinic flux above clouds will increase due to scattering from the top and within the clouds,. There is some scattering downward thus increasing the actinic flux immediately below the clouds. Further below and downward to the surface, the cloud the actinic flux is reduced. The presence of aerosols in the lowest kilometer has little or no effect above them, but further reduces the actinic flux in the lowest kilometer. Multiple layers of clouds will increase the actinic flux above and in-between the clouds, but further reduces the actinic flux in the lowest kilometer. The effect of cloud optical depth (COD) on actinic flux and *j*-values becomes smaller (smaller percent change per COD) as the COD increases. In the CAMx model, COD less than 5 is treated the same regardless of the value of COD.

We compared the cloud category from the NAM and GFS MOS forecasts with that observed from the GOES Surface and Insolation Products. We found that a high percentage of the MOS "clear" and "overcast" cloud forecasts validated in those respective categories. However, MOS cloud forecasts of "few", "scattered", and "broken" had equal chances of validating in any of the five cloud categories. We found that there is a difference in the diurnal characteristics of the MOS forecast clouds and that observed in the GSIP. We are not 100% certain that the GSIP observations are not biased or have a diurnal preference.

7. Recommendations

Ozone profile effects on UV photolysis are not large at high sun, but the effects at low sun during commuting hours can be significant. The fix is relatively easy within CAMx by regenerating the clear-sky look-up table using climatological ozone profiles more representative within Texas. There are several possible sources for ozone profiles in this region from satellite measurements to ground-based measurements, e.g. NEUBrew Network. We recommend that a better ozone profile climatology be used rather than the USSA standard ozone profile. One suggested profile climatology is the SBUV/2 ozone *a prior* ozone profile used for the version 8.0 processing. This ozone profile climatology is variable with latitude, total ozone amount and month. This profile climatology is used for stratospheric ozone profiles and it is uncertain whether the ozone profile below the tropopause will be directly usable for air quality applications.

We recommend that support for additional aerosol studies be considered. Even with the great amount of literature on aerosols, there is still a lack of information about aqueous or chemically derived aerosols and their scattering properties. Also, there is very little information about the variability with height of the various aerosols. We don't know enough about the aerosol profile given its source and type. The USDA has four stations within Texas from which aerosol optical depth and single scattering albedo can be derived. A cloud-screening procedure was applied to the USDA aerosol+cloud optical depth but further refinement in the algorithm is needed. There is already enough information archived to determine statistics about the aerosol properties at these sites.

We noted that in the CAMx model that cloud optical depths of 5 or less were treated as if they had an optical depth of 0. Our sensitivity studies show a large change in $j(O_3)$ between cloud

optical depths of 0 and 5. The increase in scattered radiation above optically thin clouds is non-trivial and can lead to large increases in ozone above low clouds.

Clouds have the greatest impacts upon the amount of radiation available to generate tropospheric ozone. Therefore errors in the forecast of clouds translate into errors in the ozone forecast. Given a forecast of cloud amount and cloud height from the MOS forecasts do not provide enough information about the cloud's optical depth and extent of the cloud field. We suggest contacting the CIMSS/SSEC at the University of Wisconsin as this group has performed research and applications of cloud forecasting by moving clouds in GOES imager with model forecast wind streamlines. This group may have other suggestions about utilizing GOES imagery in a forecast. The GSIP cloud product used in this study has a 3-4 hour post observation delivery time.

7. References

Anderson, G., Clough, S., Krneizyz, F., Chetwynd, J., Shettle, A. (1986). AFGL atmospheric constituent profiles. AFGL Technical Report. Bedford, MA, Air Force Geophysical Laboratory.

Augustine, J., G. Hodges, E. Dutton, J. Michalsky, and C. Cornwall, An aerosol optical depth climatology for NOAA's national surface radiation budget network (SURFRAD), *J. Geophys. Res.*, **113**, D11204, doi:10.1029/2007JD009504, 2008.

Bruhl, C. and P. J. Crutzen (1989). "On the Disproportionate Role of Tropospheric Ozone as a Filter against Solar Uv-B Radiation." Geophysical Research Letters **16**(7): 703-706

Cooper, O. R., D. D. Parrish, et al. (2010). "Increasing springtime ozone mixing ratios in the free troposphere over western North America." Nature **463**(7279): 344-348.

Cooper, O. R., A. Stohl, et al. (2006). "Large upper tropospheric ozone enhancements above midlatitude North America during summer: In situ evidence from the IONS and MOZAIC ozone measurement network." Journal of Geophysical Research-Atmospheres **111**(D24): -.

Dickerson, R. R., S. Kondragunta, et al. (1997). "The impact of aerosols on solar ultraviolet radiation and photochemical smog." Science **278**(5339): 827-830.

Elterman, L., Aerosol Measurements in the Troposphere and Stratosphere, Applied Optics, Vol 5, Num 11, pp 1769-1775, 1996.

Fruh, B., E. Eckstein, et al. (2003). "Ground-based measured and calculated spectra of actinic flux density and downward UV irradiance in cloudless conditions and their sensitivity to aerosol microphysical properties." Journal of Geophysical Research-Atmospheres **108**(D16): -.

He, S. and G. R. Carmichael (1999). "Sensitivity of photolysis rates and ozone production in the troposphere to aerosol properties." Journal of Geophysical Research-Atmospheres **104**(D21): 26307-26324.

Jacobson, M. Z. (1998). "Studying the effects of aerosols on vertical photolysis rate coefficient and temperature profiles over an urban airshed." Journal of Geophysical Research-Atmospheres **103**(D9): 10593-10604.

Junkermann, W., C. Bruhl, et al. (2002). "Actinic radiation and photolysis processes in the lower troposphere: Effect of clouds and aerosols." Journal of Atmospheric Chemistry **42**(1): 413-441.

Kazantzidis, A., A. F. Bais, D.S. Balis, E. Kosmidis, C. S. Zerefos (2005). "Sensitivity of solar UV radiation to ozone and temperature profiles at Thessaloniki, Greece." Journal of Atmospheric and Solar-Terrestrial Physics **67**: 1321-1330.

Krzyscin, J. W. (2000). "Impact of the ozone profile on the surface UV radiation: Analyses of the Umkehr and UV measurements at Belsk (52 degrees N, 21 degrees E), Poland." Journal of Geophysical Research-Atmospheres **105**(D4): 5009-5015.

Lapeta, B., O. Engelsen, et al. (2000). "Sensitivity of surface UV radiation and ozone column retrieval to ozone and temperature profiles." Journal of Geophysical Research-Atmospheres **105**(D4): 5001-5007.

Lantz, K. O., R. E. Shetter, et al. (1996). "Theoretical, actinometric, and radiometric determinations of the photolysis rate coefficient of NO2 during the Mauna Loa observatory photochemistry experiment 2." Journal of Geophysical Research-Atmospheres **101**(D9): 14613-14629.

Laszlo, I, J. D. Tarpley and R. T. Pinker,(2002), A comparison of surface solar fluxes in the NOAA operational GOES SRB product with those derived from the ISCCP D1 data. AMS 11th Conference on Atmospheric Radiation, June 3-7, 2002, Ogden, Utah.

Lefer, B. L., R. E. Shetter, et al. (2003). "Impact of clouds and aerosols on photolysis frequencies and photochemistry during TRACE-P: 1. Analysis using radiative transfer and photochemical box models." Journal of Geophysical Research-Atmospheres **108**(D21): -.

Liao, H., Y. L. Yung, et al. (1999). "Effects of aerosols on tropospheric photolysis rates in clear and cloudy atmospheres." Journal of Geophysical Research-Atmospheres **104**(D19): 23697-23707.

Liu, S. C., S. A. Mckeen, et al. (1991). "Effect of Anthropogenic Aerosols on Biologically-Active Ultraviolet-Radiation." Geophysical Research Letters **18**(12): 2265-2268

Madronich, S. (1992). "Implications of Recent Total Atmospheric Ozone Measurements for Biologically-Active Ultraviolet-Radiation Reaching the Earths Surface." Geophysical Research Letters **19**(1): 37-40.

McKenzie, R., D. Smale, et al. (2003). "Ozone profile differences between Europe and New Zealand: Effects on surface UV irradiance and its estimation from satellite sensors." Journal of Geophysical Research-Atmospheres **108**(D6): -.

Schwander, H., P. Koepke, et al. (1997). "Uncertainties in modeled UV irradiances due to limited accuracy and availability of input data." Journal of Geophysical Research-Atmospheres **102**(D8): 9419-9429.

Tsay, S. C. and K. Stamnes (1992). "Ultraviolet-Radiation in the Arctic - the Impact of Potential Ozone Depletions and Cloud Effects." Journal of Geophysical Research-Atmospheres **97**(D8): 7829-7840.

Tang, Y. H., G. R. Carmichael, et al. (2003). "Impacts of aerosols and clouds on photolysis frequencies and photochemistry during TRACE-P: 2. Three-dimensional study using a regional chemical transport model." Journal of Geophysical Research-Atmospheres **108**(D21): -.